Frontiers of Plasma Physics in the Solar Wind

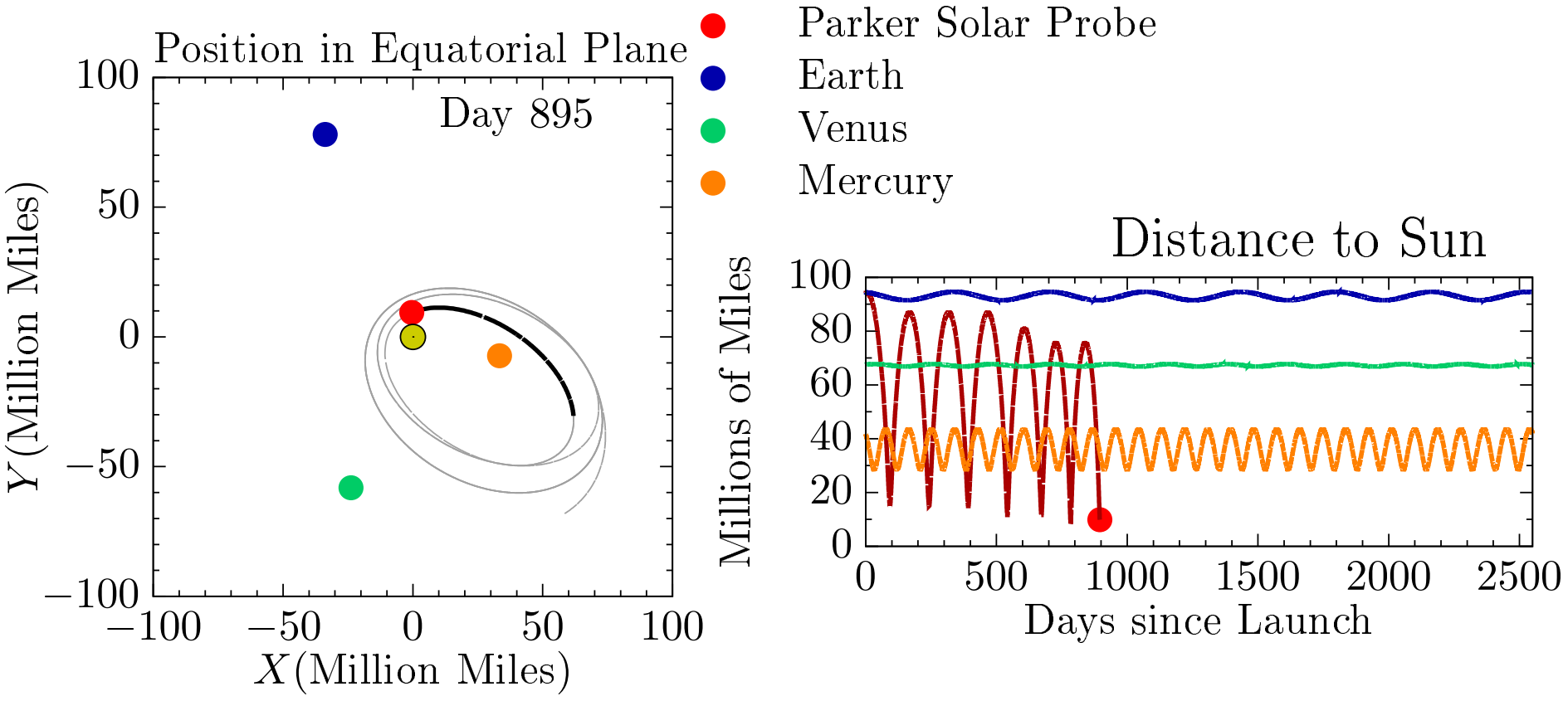

Kristopher G. Klein
GPAP Summer School
20 June, 2019

THE UNIVERSITY OF ARIZONA
COLLEGE OF SCIENCE
LUNAR & PLANETARY LABORATORY

Parker's Solar Wind Solution (1958)

Combining momentum, continuity, and an isotropic temperature with a bit of elbow grease yields

$$\frac{1}{u}\frac{du}{dr}\left(u^2 - \frac{2T}{m_p}\right) = \frac{4T}{m_p r} - \frac{GM_\odot}{r^2}.$$

Parker's Solar Wind Solution (1958)

Combining momentum, continuity, and an isotropic temperature with a bit of elbow grease yields

$$\frac{1}{u}\frac{du}{dr}\left(u^2 - \frac{2T}{m_p}\right) = \frac{4T}{m_p r} - \frac{GM_\odot}{r^2}.$$

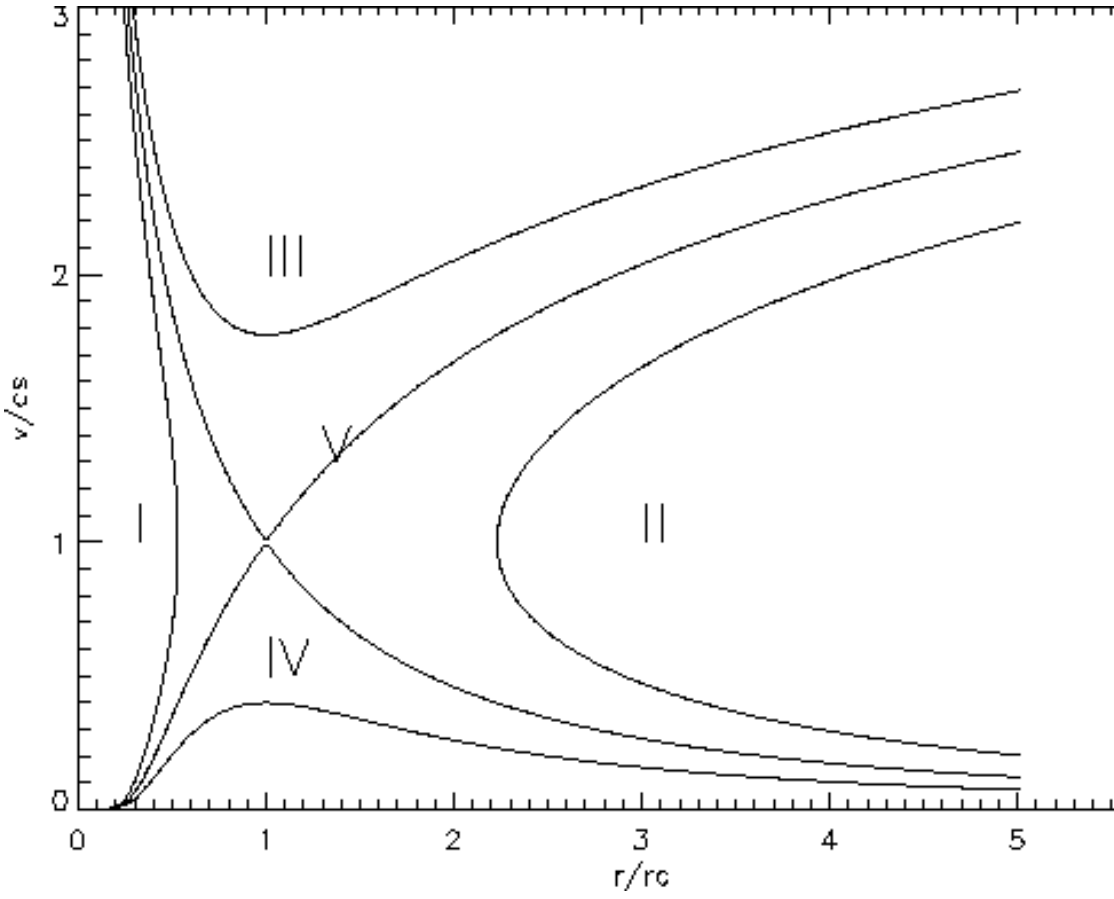

There are five types of solutions predicted by the original model; only one matched physical restrictions near and far from the Sun, a super-sonic **solar wind** (V).

However, there were no observations of a several hundred mile per second flow of plasma past the Earth.

The First Observations of the Solar Wind

The recorded proton currents can apparently be related to the corpuscular emission of the sun; this emission has thus been observed for the first time in the interplanetary space outside the magnetic field of the earth.
Gringauz et al. (1960) Luna 1

[T]he plasma velocity . . . appears to be greater than that observed close to the earth by Explorer X. The measured velocity agrees fairly well with the value predicted from Parker's "solar wind" theory.
Neugebauer et al. (1962) Mariner 2

Where Have We Measured?

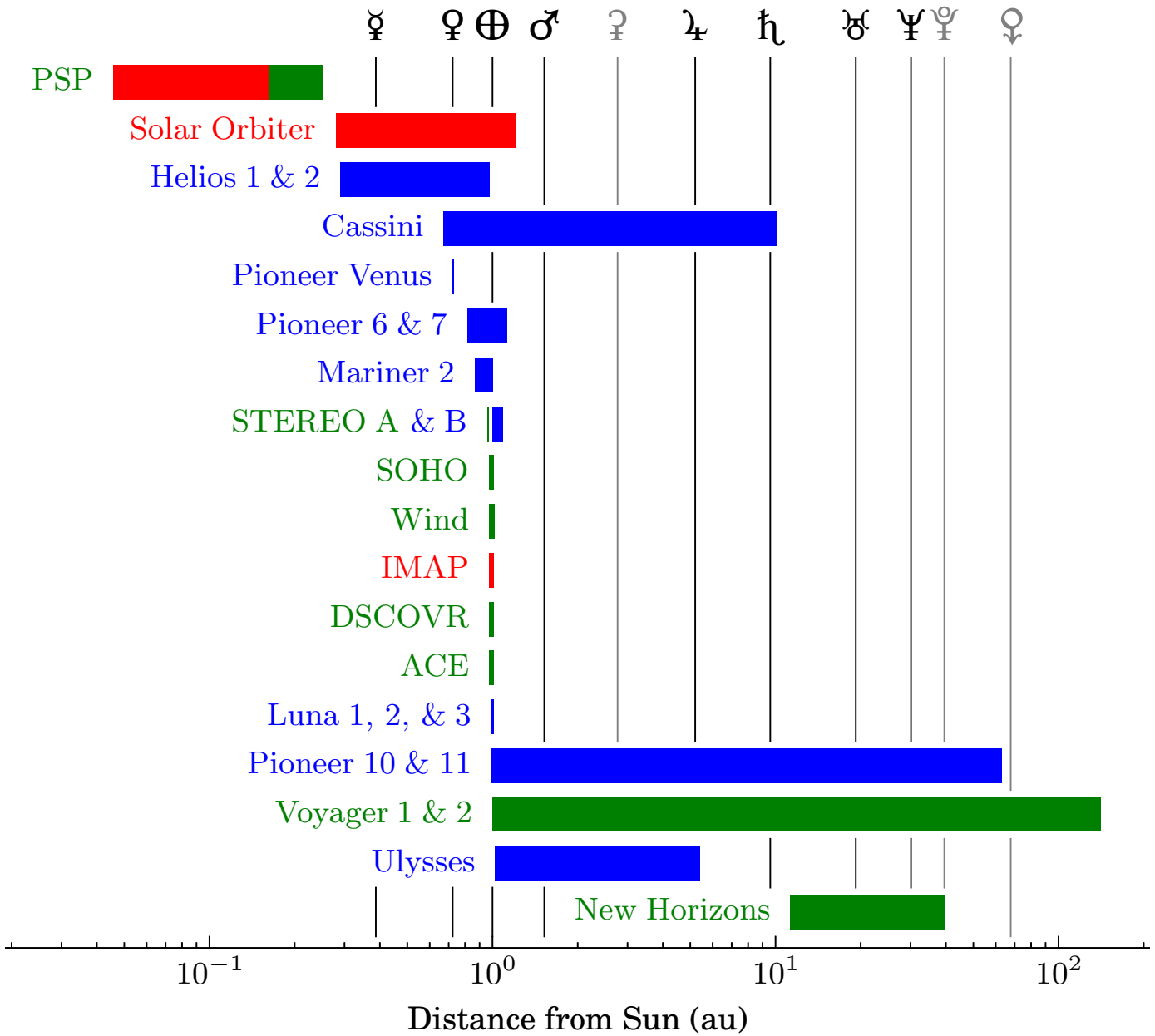

Verscharen et al `https://arxiv.org/pdf/1902.03448.pdf`

Measuring Charged Particles in the Solar Wind

Particle Velocity Distributions $f_s(\mathbf{v})$

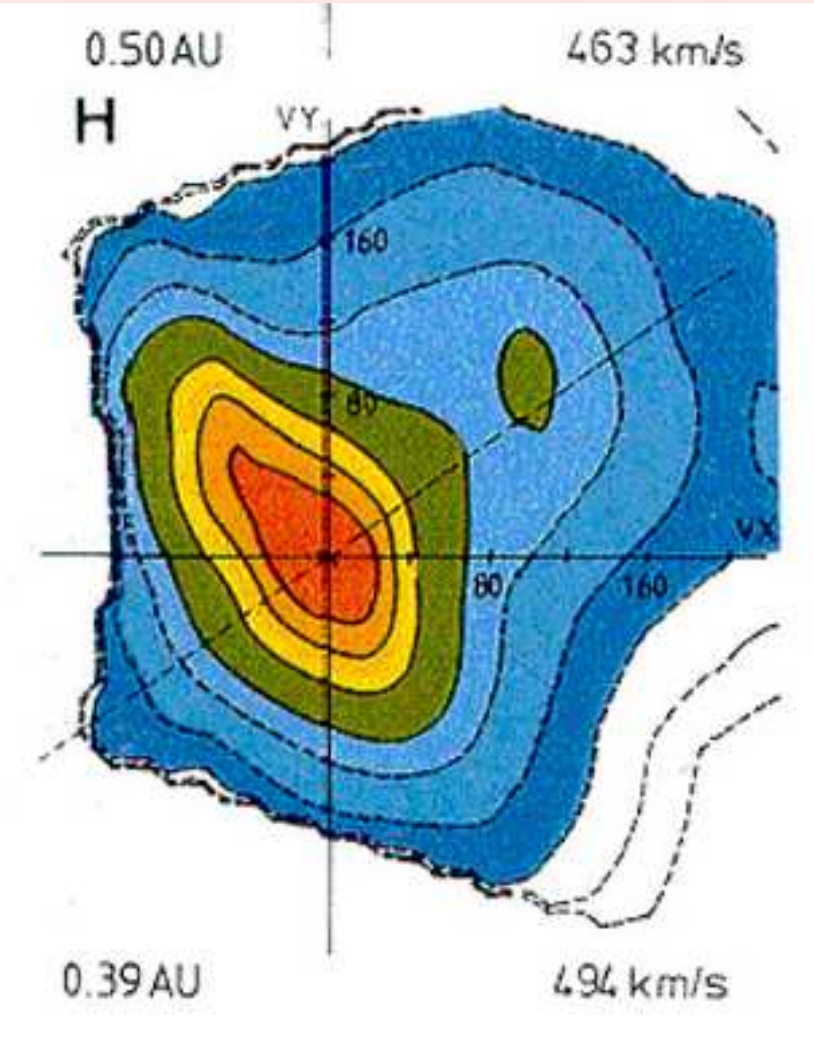

Marsch et al, 2012: Helios

Electrostatic Analyzer (ESA)

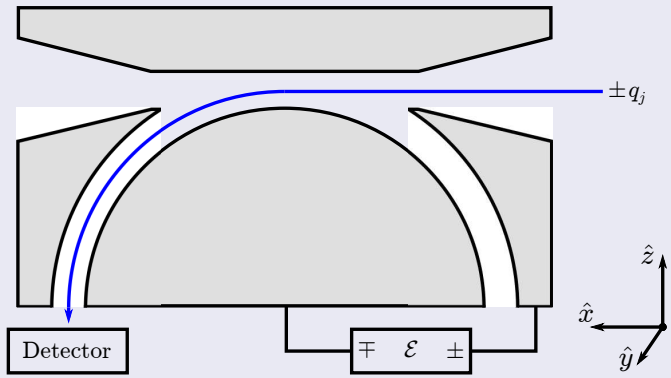

Faraday Cup

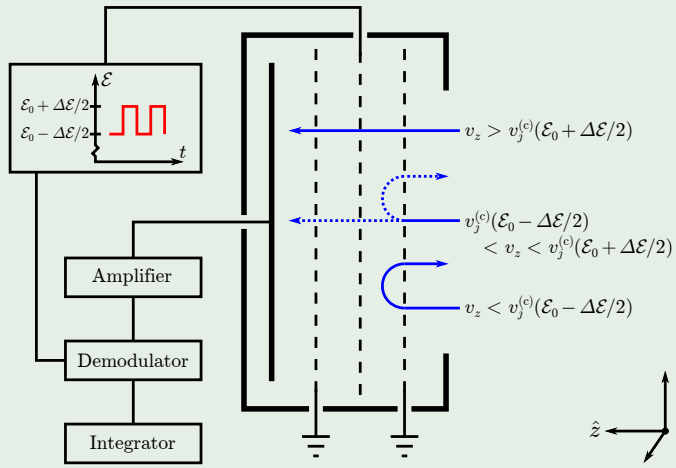

Verscharen et al, 2019

Measuring Electromagnetic Fields in the Solar Wind

FGM

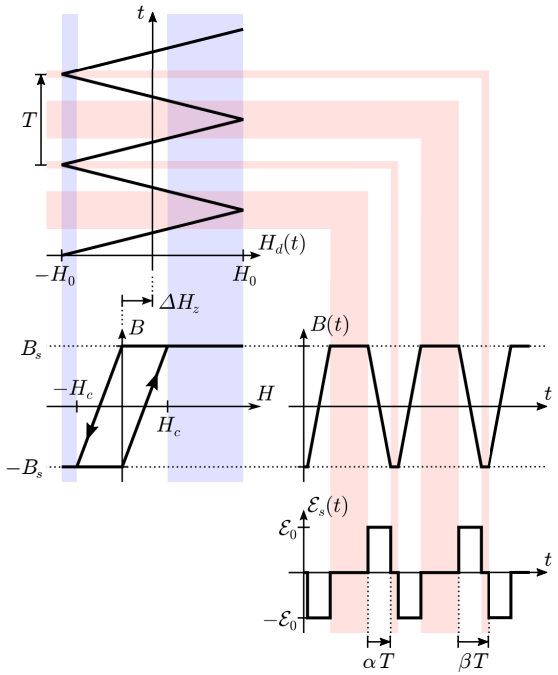

Magnetic Fields

- **Fluxgate** Magnetometers are ideal for lower frequency (< 10 Hz) measurements, exploiting the hysteresis of ferromagnetic materials using separate drive and sensing coils.
- **Search Coil** Magnetometers are optimized for higher frequency measurements, is a 'simple' coil wrapped around a core, which produces a voltage due to the change in the magnetic field.

Electric Fields

Typically measured using monopole or dipole antennas, ranging in size from 6 to 50 m. Besides, $\mathbf{E}$, also provide estimated of electron density through QTN spectra.

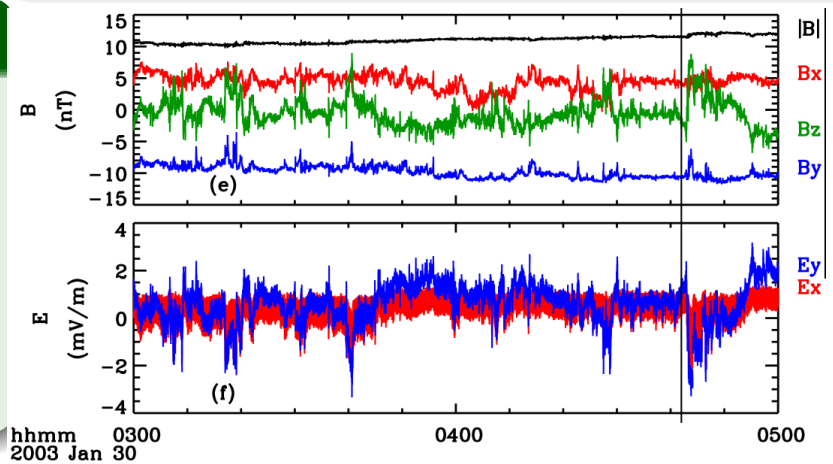

How Can We Use Departures from Equilibrium to Understand the Solar Wind?

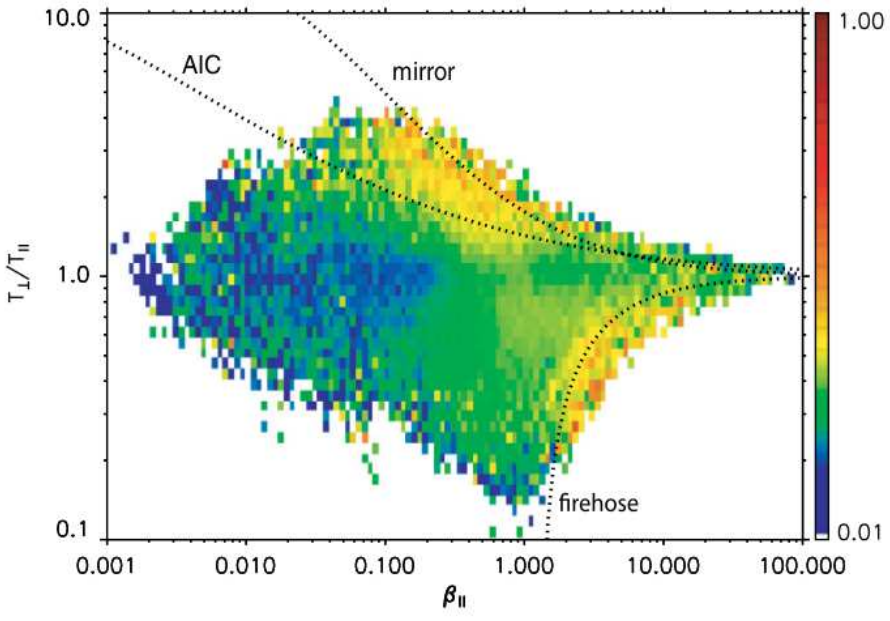

Bale et al 2009 Wind

- As Driver of Dynamics
- As Diagnostic of Remote Processes

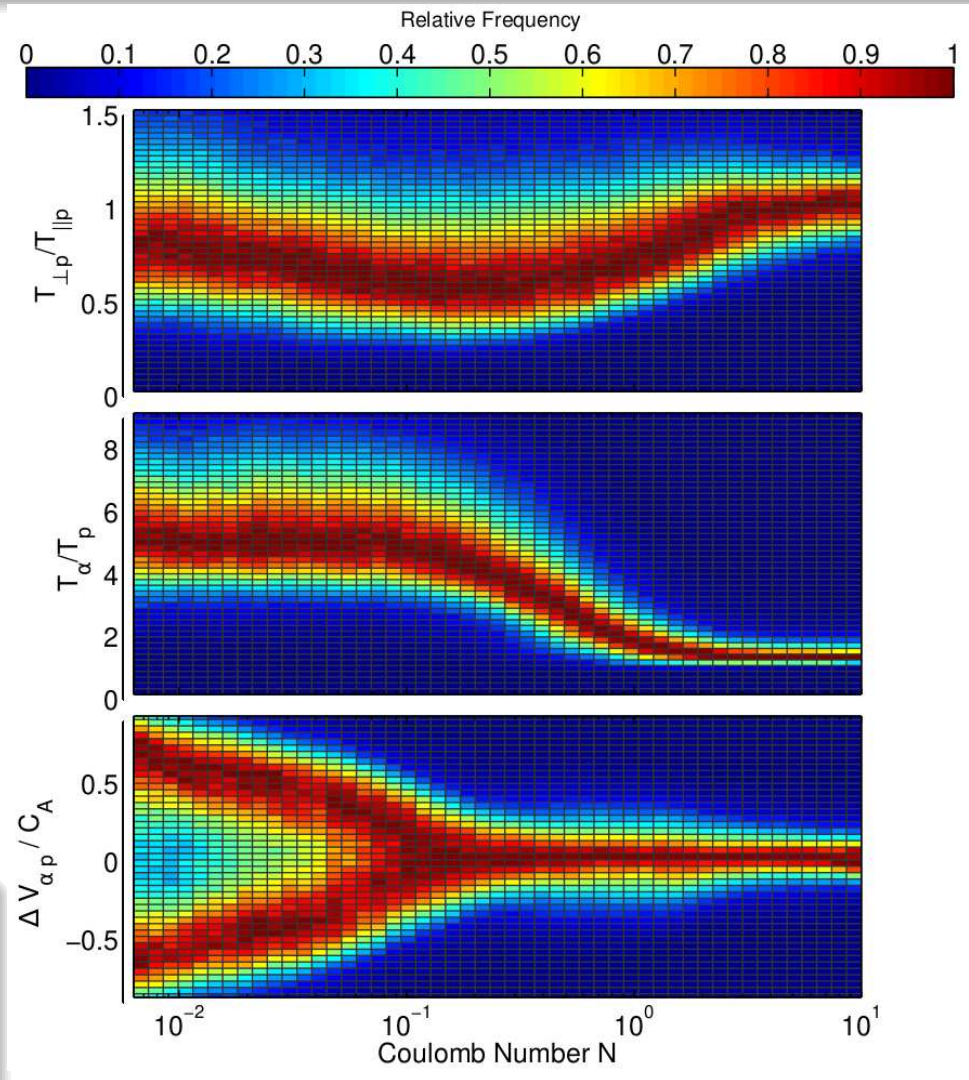

Kasper et al 2017 Wind

Extracting Energy from non-Maxwellian Distributions

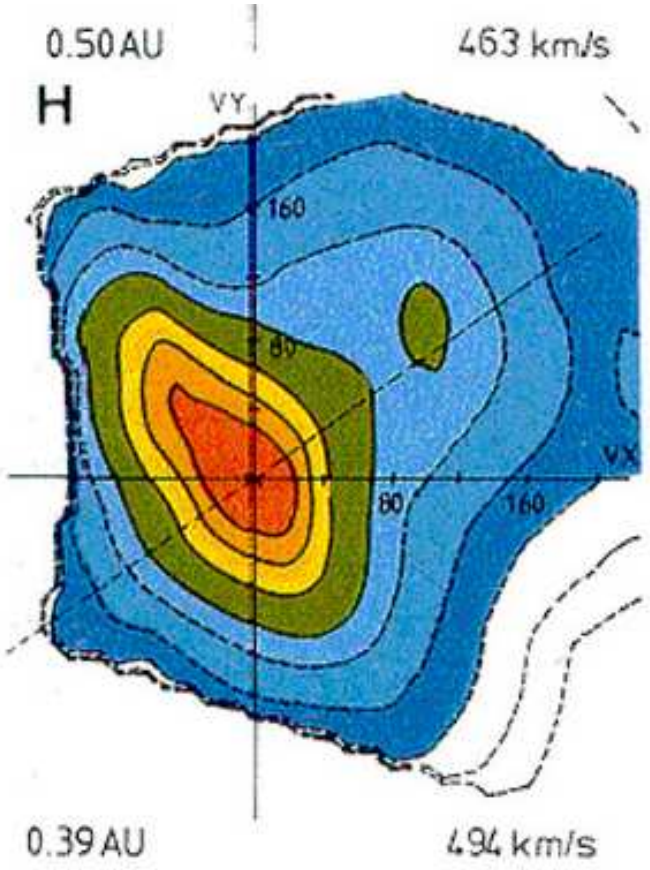

Marsch 2012 Helios

For this work, we focus only on linear stability.

Fluid Firehose Instability:

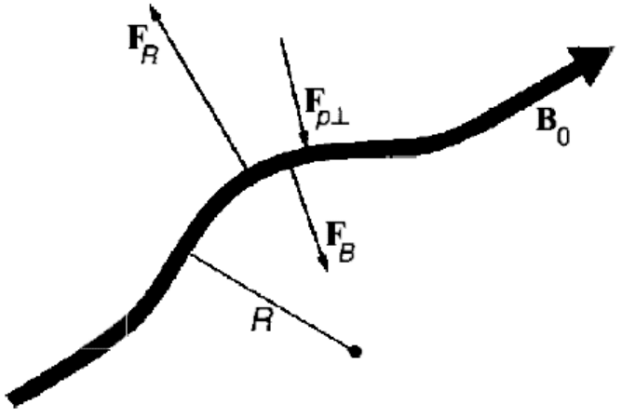

Treumann & Baumjohann, 1997

Cyclotron **Resonant** Instability:

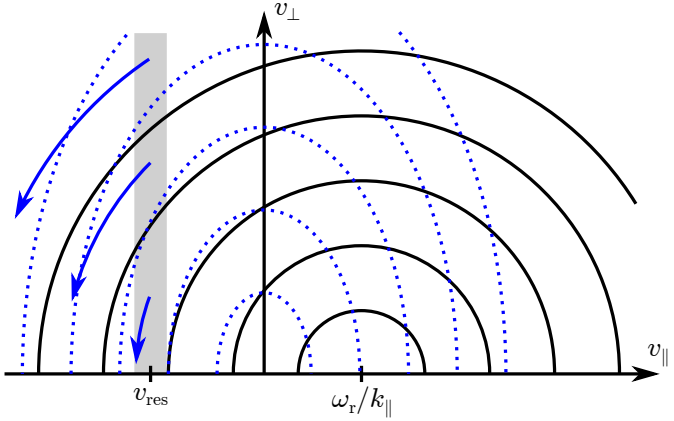

Verscharen, Klein, & Maruca, under review

Simple Models for Stability Thresholds

Focusing on a single free-energy source and assuming an analytic form for $f_p(v_\perp, v_\parallel)$, we parameterize where specific instabilities arise.

$$\frac{T_{\perp,p}}{T_{\parallel,p}} = 1 + \frac{a}{\left(\beta_{\parallel,p} - \beta_0\right)^b}$$

Hellinger et al. 2006

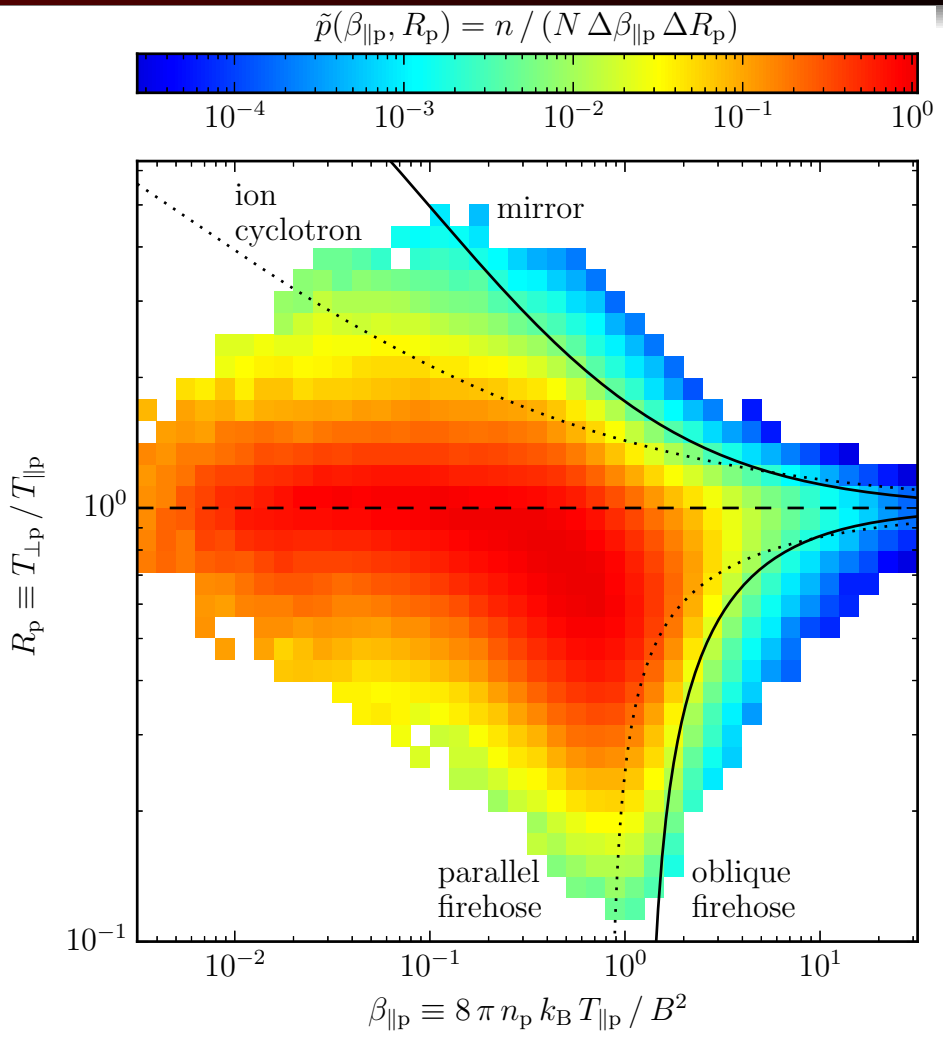

Verscharen, Klein, & Maruca, under review Wind

Such models do not account for other energy sources (e.g. other species anisotropies, relatively drifting components)

Instabilities Limit the Solar Wind's Evolution

Matteini et al 2007

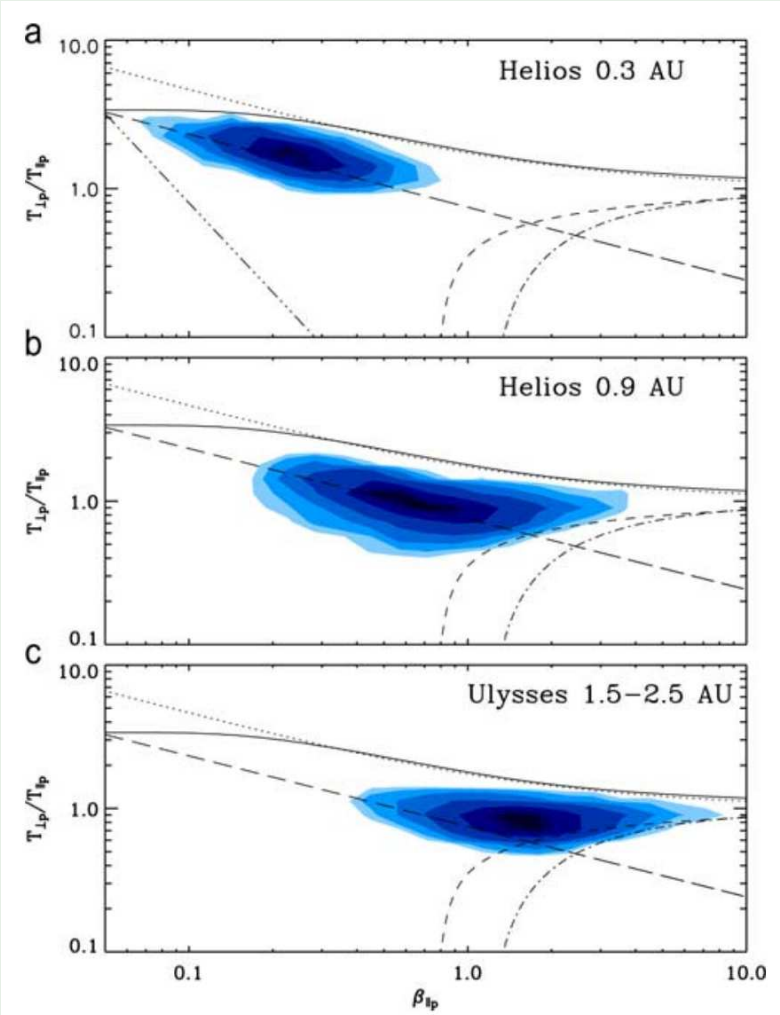

Bale et al 2009

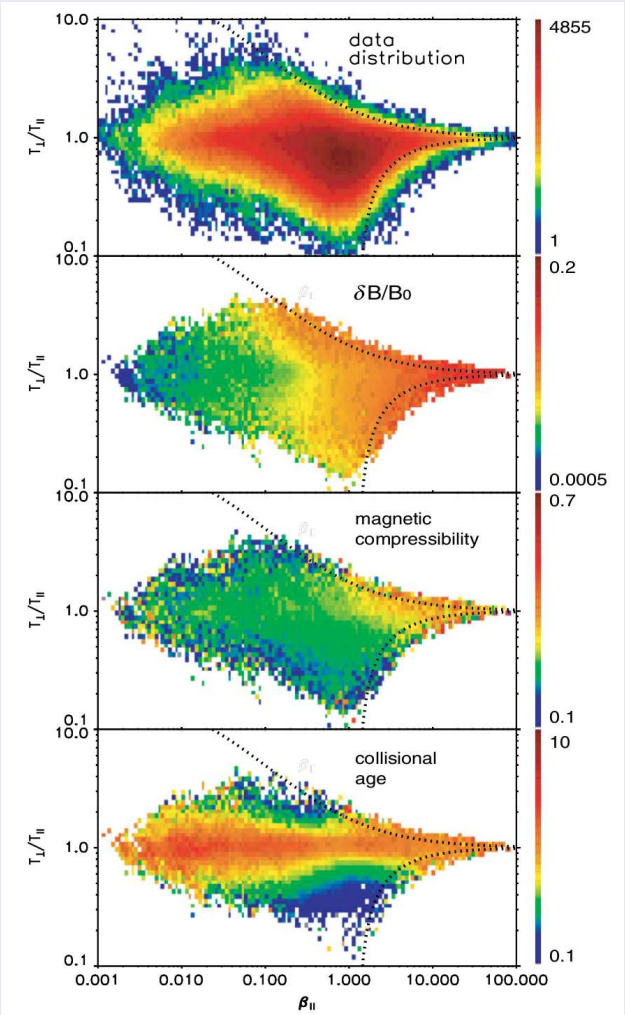

These correlations may mask underlying dependencies.

(Hellinger & Travnicek 2014)

Advanced Models for Stability Thresholds

$$\Lambda_{\text{firehose}} = \frac{\beta_{\parallel} - \beta_{\perp}}{2} + \frac{\sum_s \rho_s |\Delta \mathbf{v}_s|^2}{\rho v_A^2} > 1$$

$$\Lambda_{\text{mirror}} = \sum_s \beta_{\perp s} \left(\frac{\beta_{\perp s}}{\beta_{\parallel s}} - 1 \right) + \frac{\left(\sum_s q_s n_s \frac{\beta_{\perp s}}{\beta_{\parallel s}} \right)^2}{2 \sum_s \frac{(q_s n_s)^2}{\beta_{\parallel s}}} > 1$$

Kunz et al 2015

These models only account for configuration-space instabilities, and in the case of Λ_{mirror} neglects drifts.

A study of resonant instabilities will require other tools.

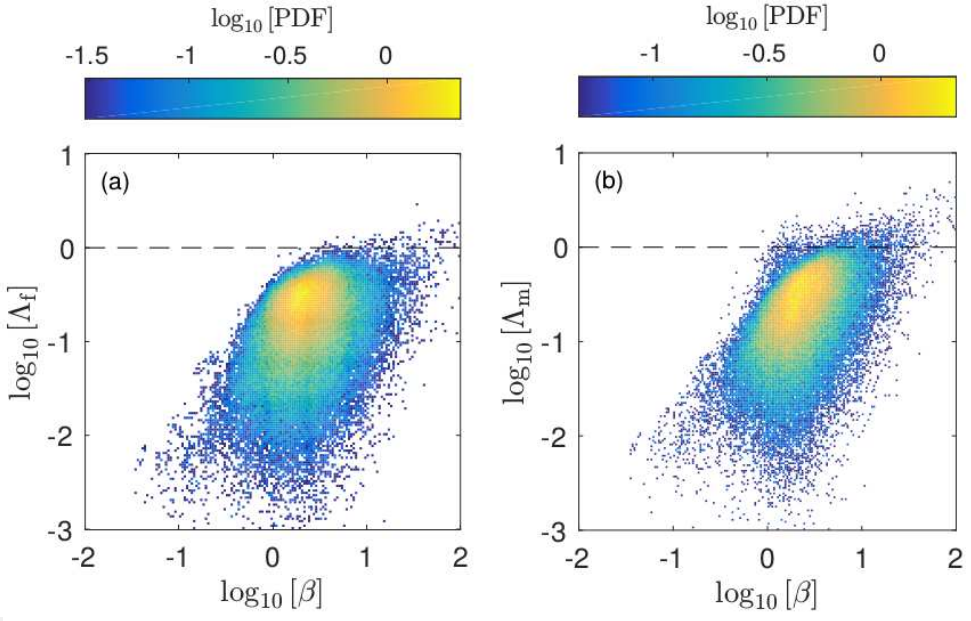

Chen et al 2016 Wind

Identifying Instabilities from Linear Dispersion Relation $|\mathcal{D}|$

Given the wave vector equation

$$\mathbf{n} \times (\mathbf{n} \times \mathbf{E}) + \underline{\epsilon} \cdot \mathbf{E} = \underline{\underline{\mathcal{D}}} \cdot \mathbf{E} = 0$$

unstable modes are solutions $|\mathcal{D}| = 0$ in complex frequency space (ω, γ) that have a positive damping rate $\gamma > 0$.

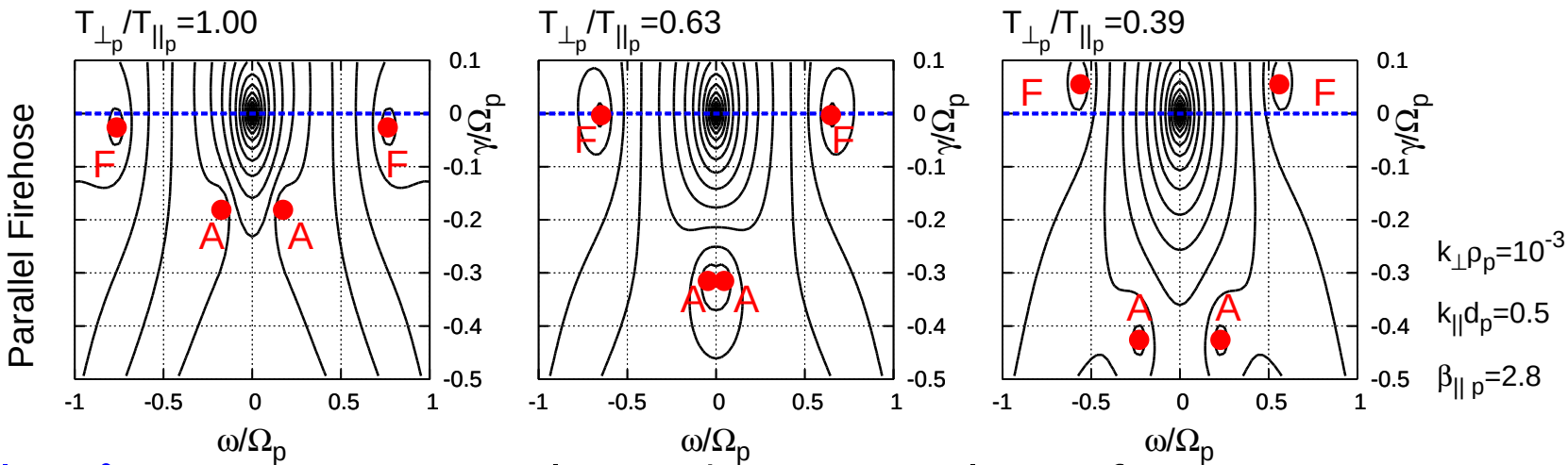

Klein & Howes 2015 Hot plasma dispersion solution from `PLUME`

Stability sensitively depends on the bulk parameters of each species, which cover a wide range of values in the solar wind, making implementing a manual scan time consuming.

The Nyquist Instability Criterion (Nyquist 1932, Penrose 1960)

Instead of searching for solutions of $|D(\omega, \gamma)| = 0$ with $\gamma > 0$, we evaluate the contour integral for the number of unstable modes:

$$W_n = \frac{1}{2\pi i} \oint \frac{d\omega}{|D(\omega, \gamma)|}.$$

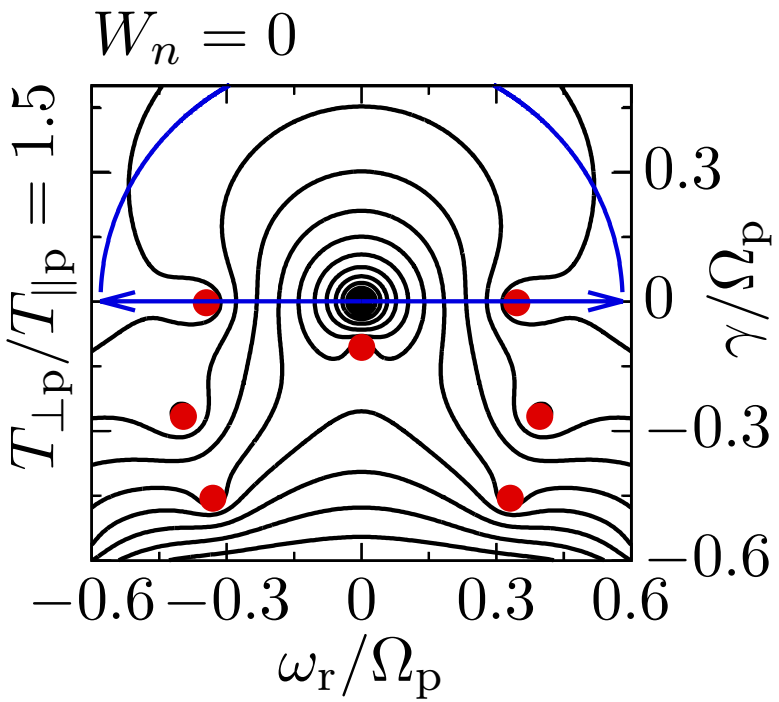

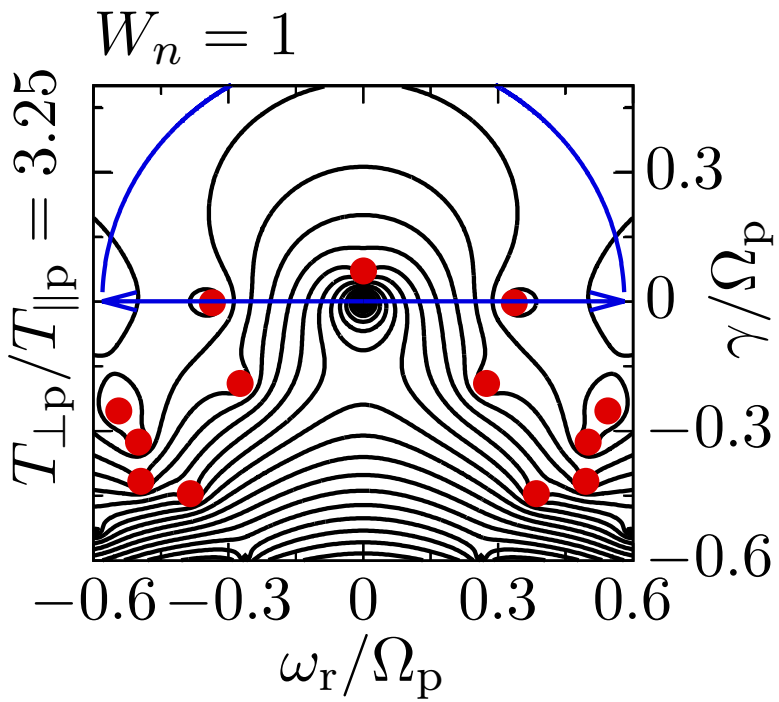

We have numerically implemented a winding number calculator using the `PLUME` dispersion solver (Klein et al. 2017 JGR).

We can test for arbitrarily fast growing modes

Instead of using $\gamma = 0$ to define the contour,
we calculate W_n for any growth rate $\gamma_{\min}$

(This requires the insertion of a branch cut).

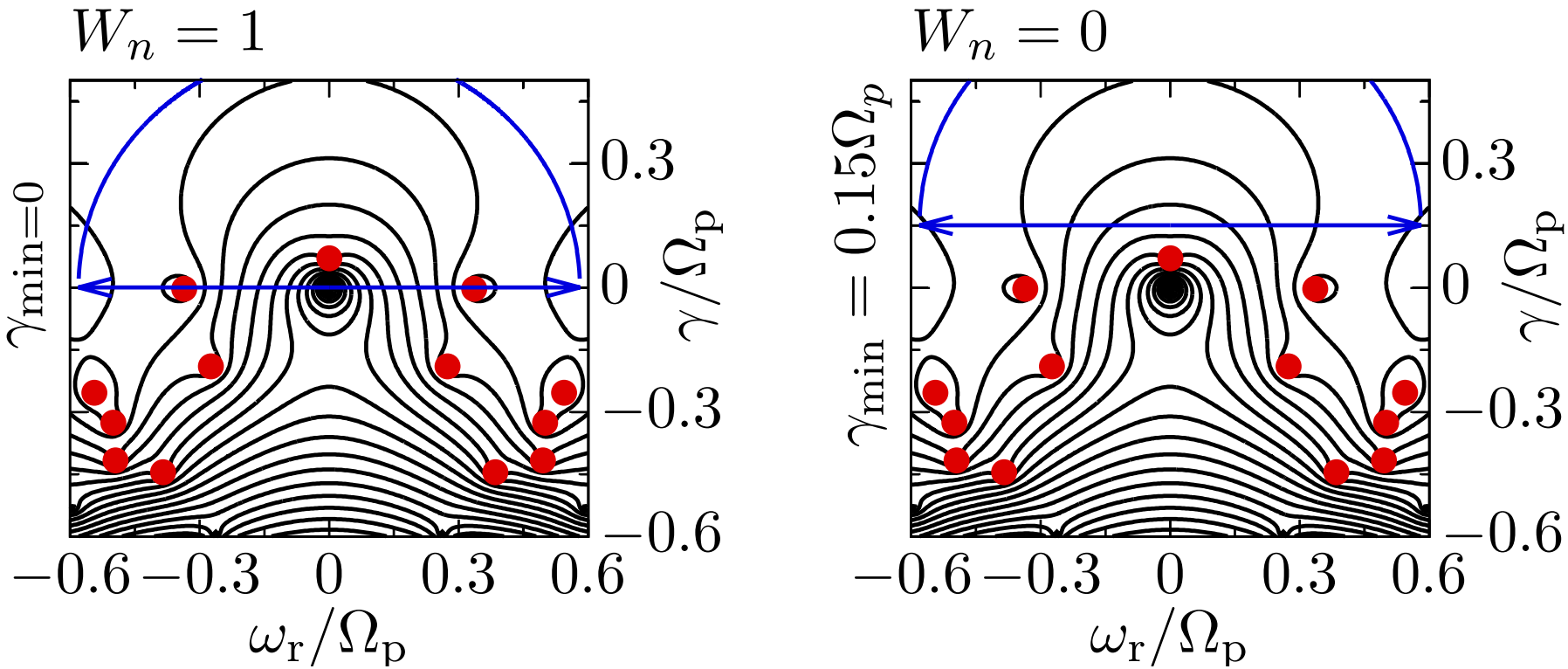

Modes with $\gamma < \gamma_{\min}$ will not be included in the calculation.

Comparisons to Actual Solar Wind Measurements

Gary et al 2016; Wind

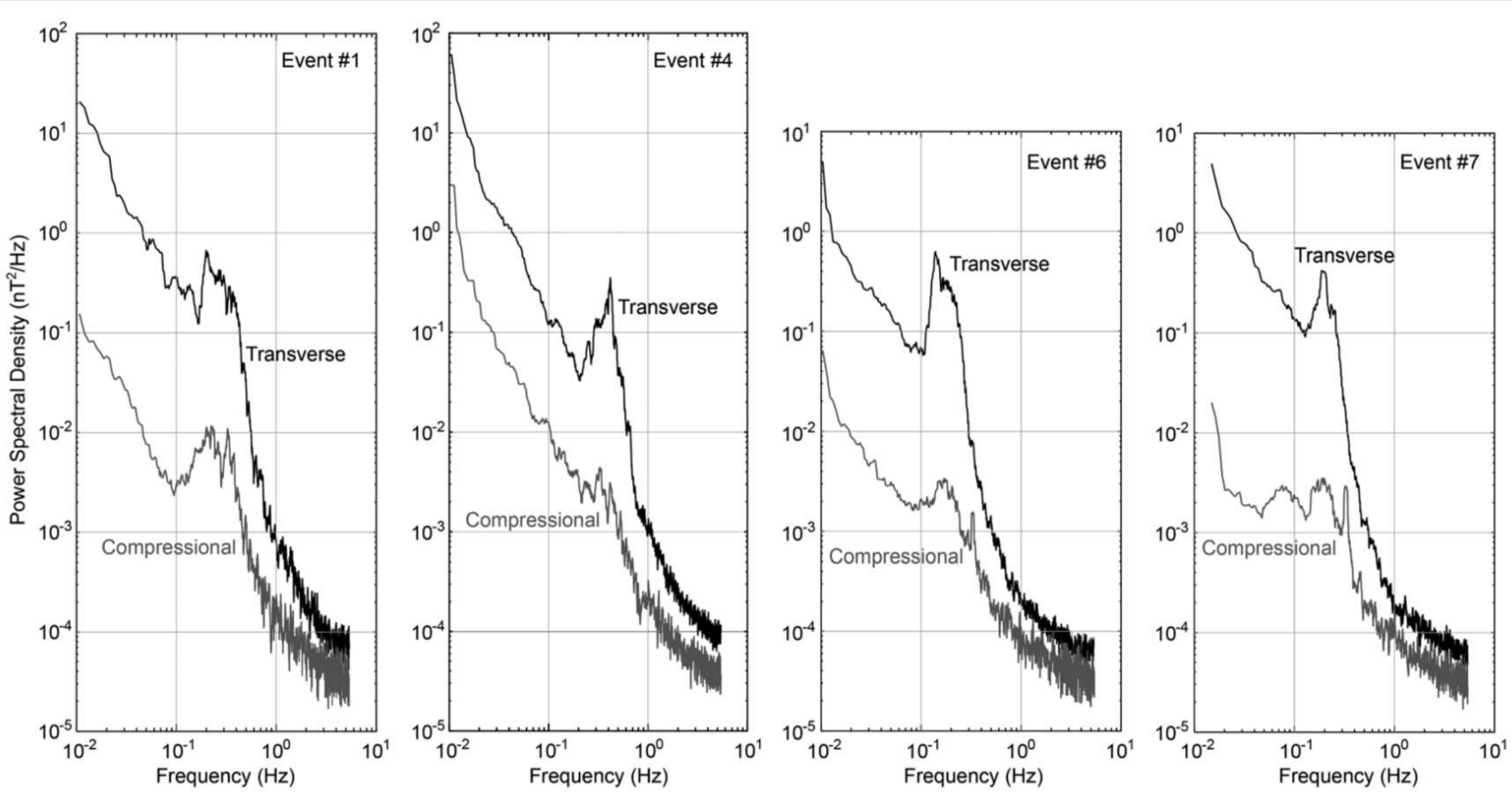

Identified 6 intervals with observational signatures of parallel propagating instabilities in the magnetic power spectra.

Do We Identify Unstable Normal Modes?

Using drifting, bi-Maxwellian moments for the proton core & beam, He^{++}, and e^{-}

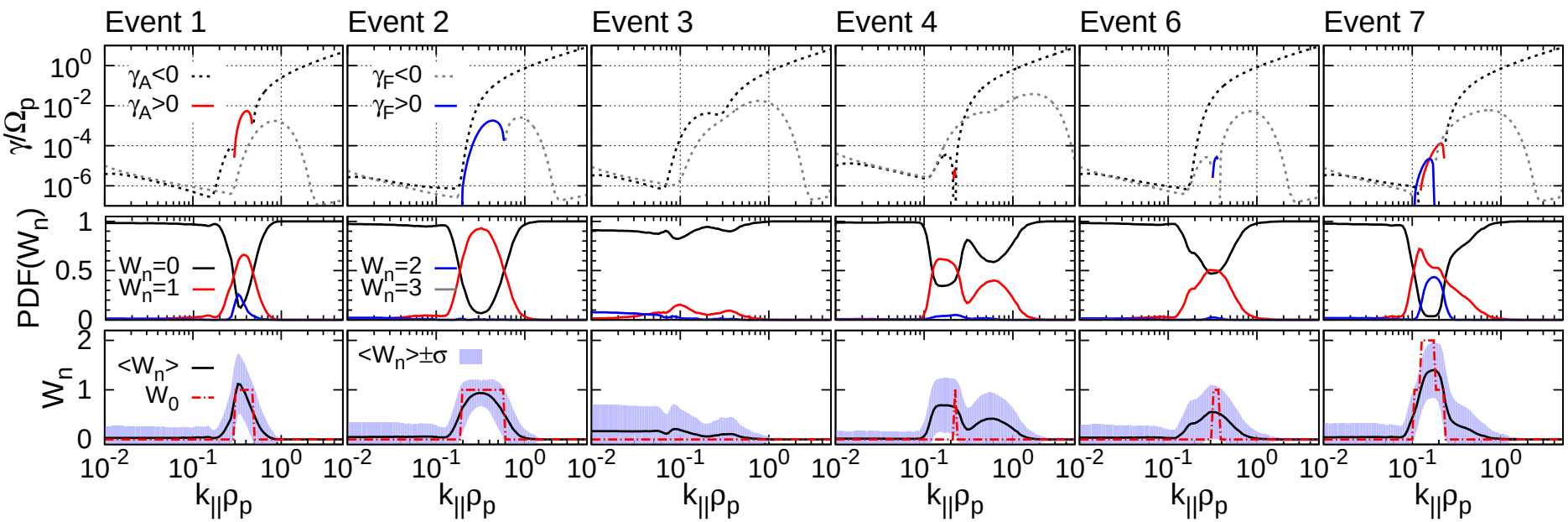

Klein et al 2017

Two events have modes with growth rates $\gamma \sim 10^{-2}\Omega_p$.

A Statistical Data Set from the Solar Wind

- We select a random set of Wind spectra, the first nominal spectra a day from 309 days in 2016 & 2017.
- For each spectrum, a nonlinear-least-squares Bi-Maxwellian fit is performed for up to three ion components;
  proton core $n_p, T_{\perp p}, T_{\parallel p}$,
  proton beam $n_b, T_{\perp b}, T_{\parallel b}, \Delta v_{pb}$,
  α **population** $n_\alpha, T_{\perp \alpha}, T_{\parallel \alpha}, \Delta v_{p\alpha}$,
  and combined with $|B|$ to produce the associated dimensionless parameters. (Klein et al 2018)

- For Each Spectra, we calculate $W_n(\mathbf{k}\rho_p)$ on a grid covering $(k_\perp, k_\parallel)\rho_p \in [10^{-2}, 10^{1}]$.
- The maximum growth rates of unstable spectra are found within $\gamma_{\min}/\Omega_p = [10^{-4}, 1]$.

Occurrence of Ion-Driven Instabilities

	# Spectra	# Unstable	Mirror	CGL FH	Kinetic
Total	309	166	14	1	151
p, b, & α	189	130	12	0	118
p & α	114	33	2	1	30
p & b	5	3	0	0	3
p	1	0	0	0	0

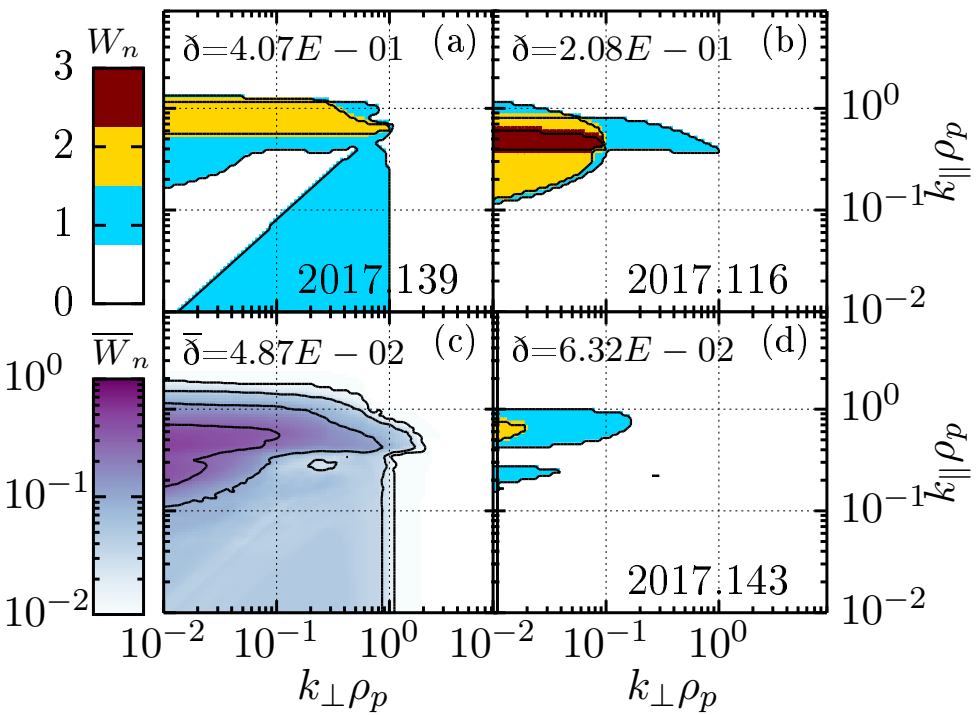

- 54% of spectra are unstable
- The majority of the instabilities are kinetic, i.e. $k_\perp\rho_p < k_\parallel\rho_p \lesssim 1$
- Instabilities preferentially arise when a proton beam is resolved

Klein et al 2018

Comparison to Other Timescales

We re-scale the stability fraction as a function of alternative timescales:

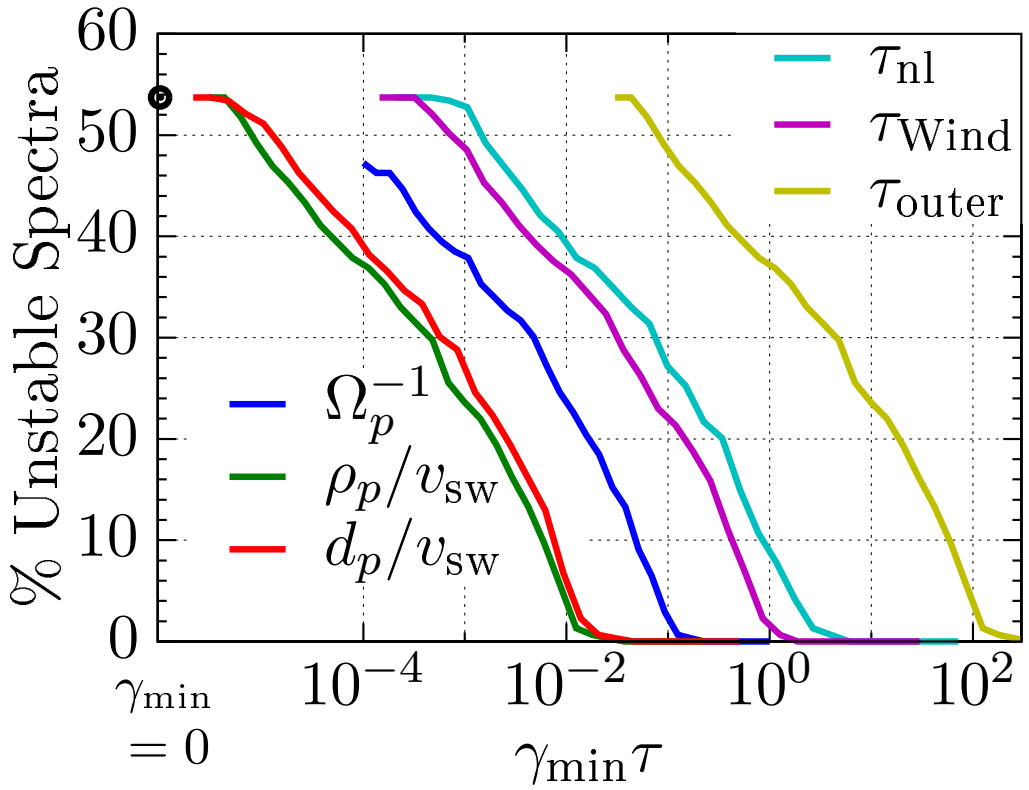

- $\frac{\rho_p}{v_{\rm sw}} = \frac{w_{\perp,p}}{\Omega_p v_{\rm sw}}$
- $\frac{d_p}{v_{\rm sw}} = \frac{v_A}{\Omega_p v_{\rm sw}}$
- $\tau_{\rm Wind} = 92{\rm s}$
- $\tau_{\rm nl} = (k_0\rho_p)^{1/3}\frac{\rho_p}{v_A}$
- $\tau_{\rm outer} = \frac{L_0}{v_{\rm sw}} = \frac{2\pi}{k_0 v_{\rm sw}}$

- The ion-kinetic timescales and $\tau_{\rm Wind}$ are faster than γ
- 10% of the spectra have γ comparable to the cascade time at $k_\perp\rho_p = 1$.

Comparing To Temperature Anisotropy Thresholds

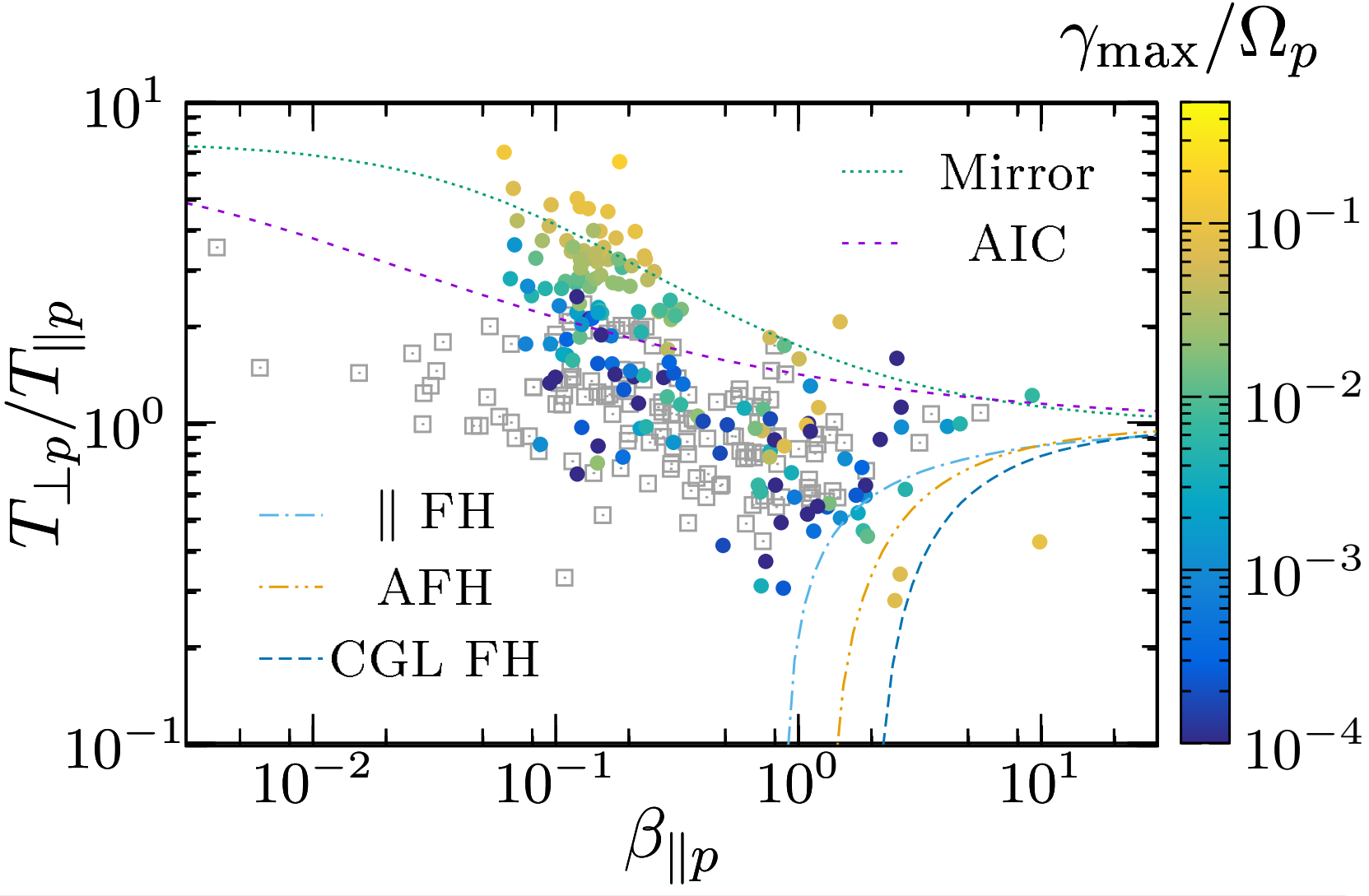

A significant fraction of spectra in the 'stable' region support growing modes. (Klein et al 2018)

ALPS: Extending beyond bi-Maxwellians

Arbitrary **L**inear **P**lasma **S**olver (`ALPS`, Verscharen et al 2018, JPP) solves the full hot-plasma dispersion relation for a set of plasma populations with **arbitrary** velocity distributions defined on a grid in momentum space.

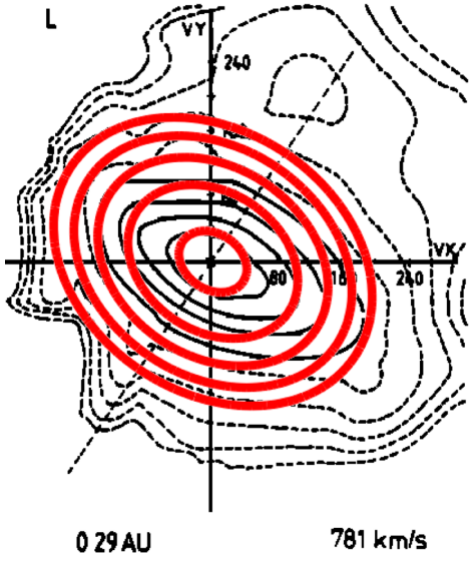

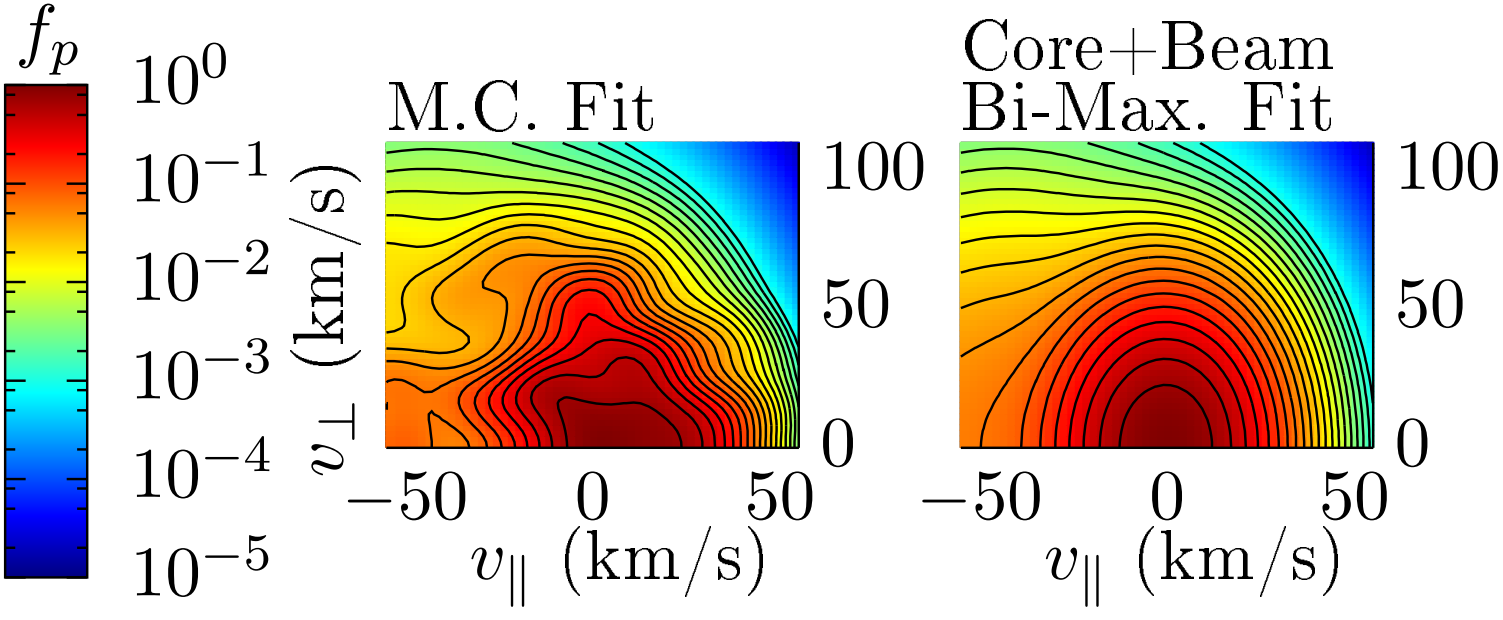

Diagnosing Remote Plasma Processes

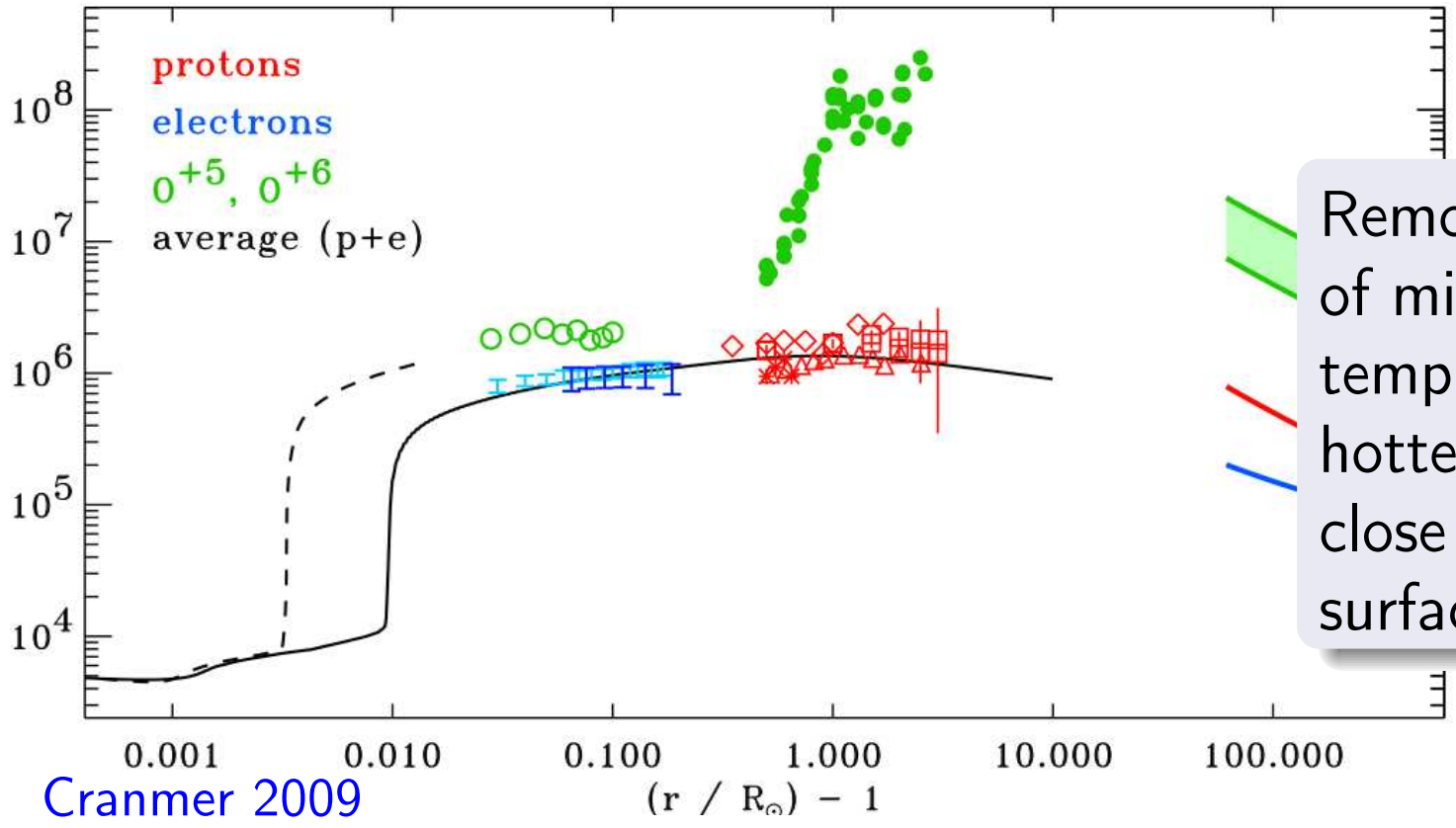

Cranmer 2009

Remote observations of minor ions indicate temperatures 10x hotter than protons close to the Sun's surface

What Mechanisms Act to Preferentially Heat Minor Ions?
And Where Do They Operate?

'Collisionality' Organizes Non-Equilibrium Structure

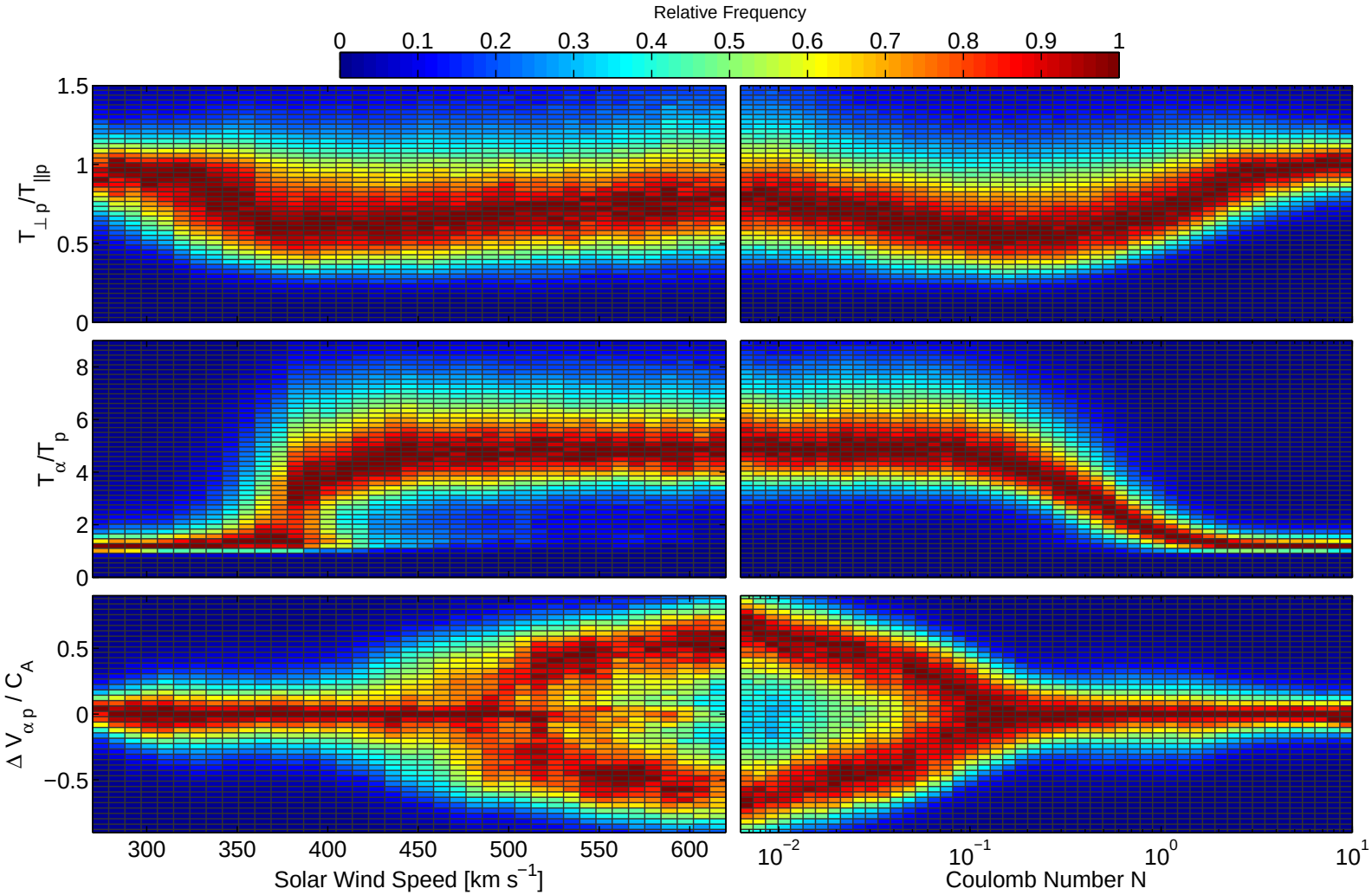

Kasper et al, 2017: Wind

$$\nu_{a,b} \approx 4\pi \frac{q_a^2 q_b^2 n_b \ln \Lambda}{m_a^2 w_b^3} \propto nT^{-3/2} \; ; \; N_c = \nu_{a,b} \frac{R}{V_{sw}}$$

$T_\alpha/T_p(N_c)$ Suggests Collisional Thermalization

Considering the evolution of temperature differences in the absence of any effects other than Coulomb collisions, keeping T_p constant, and following Spitzer (1962), we can write

$$\frac{d(T_\alpha/T_p)}{dt} = -\nu_{\alpha,p}\frac{T_\alpha}{T_p}$$

$$\rightarrow$$

$$\frac{T_\alpha}{T_p} \sim \exp\left[-\int \nu_{\alpha,p} dt\right]$$

$$\sim \exp\left[-N_c\right]$$

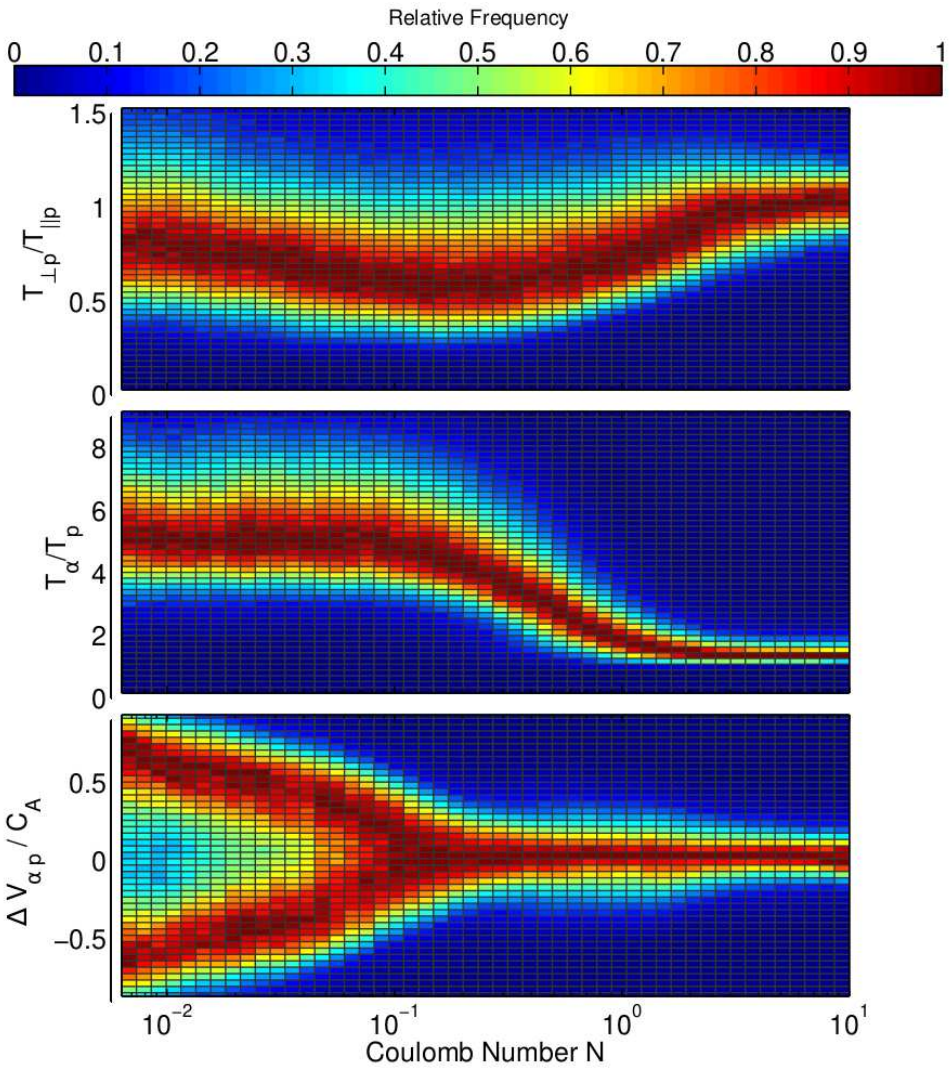

Kasper et al 2017 Wind

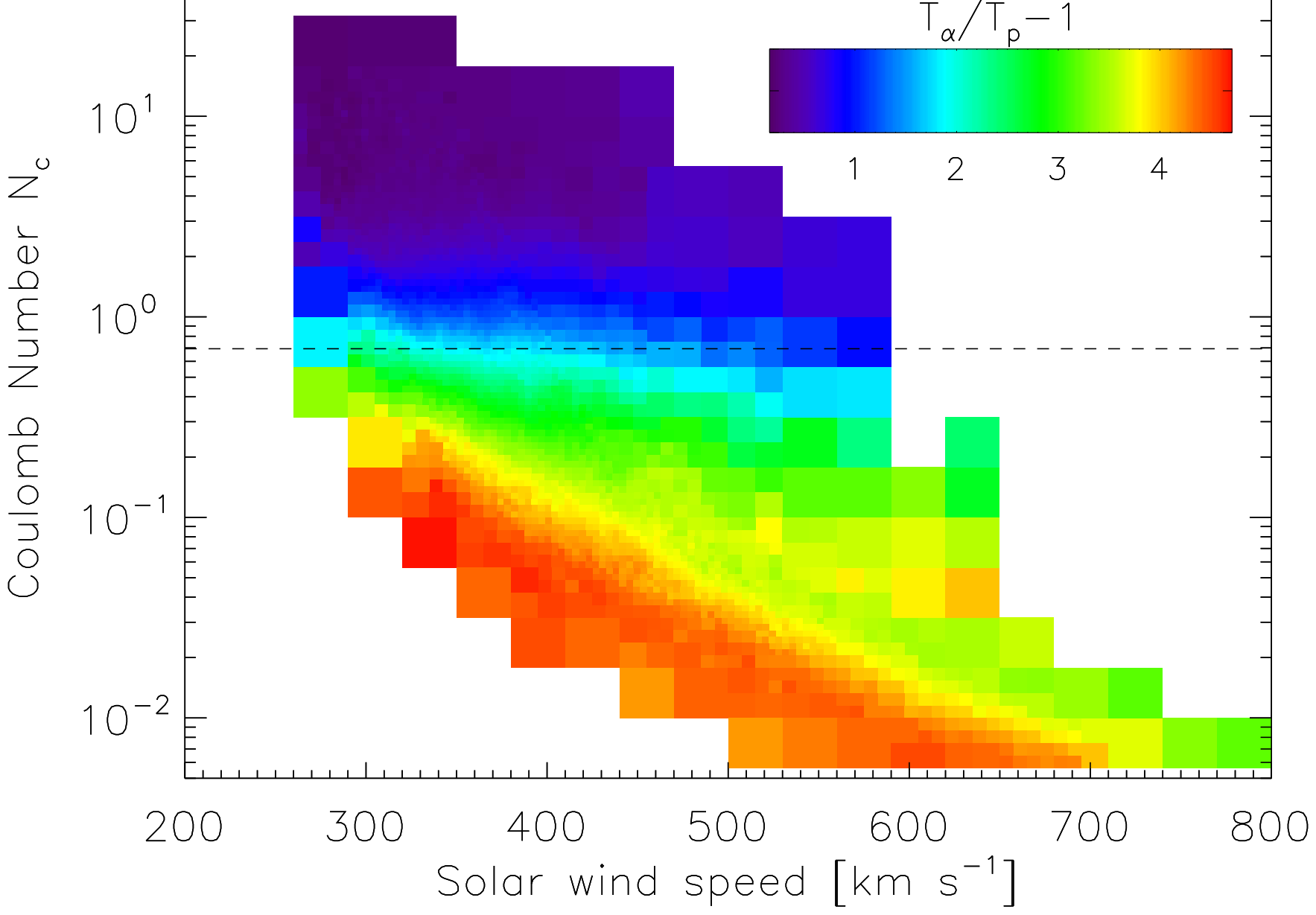

An exponential decay of $\epsilon \equiv T_\alpha/T_p - 1$ as a function of $N_c = \nu_{a,b}\frac{R}{V_{sw}}$ is seen for all V_{sw}. (Kasper et al 2017)

We assume all **preferential** heating of minor ions occurs within some zone, below a distance R_b from the Sun.

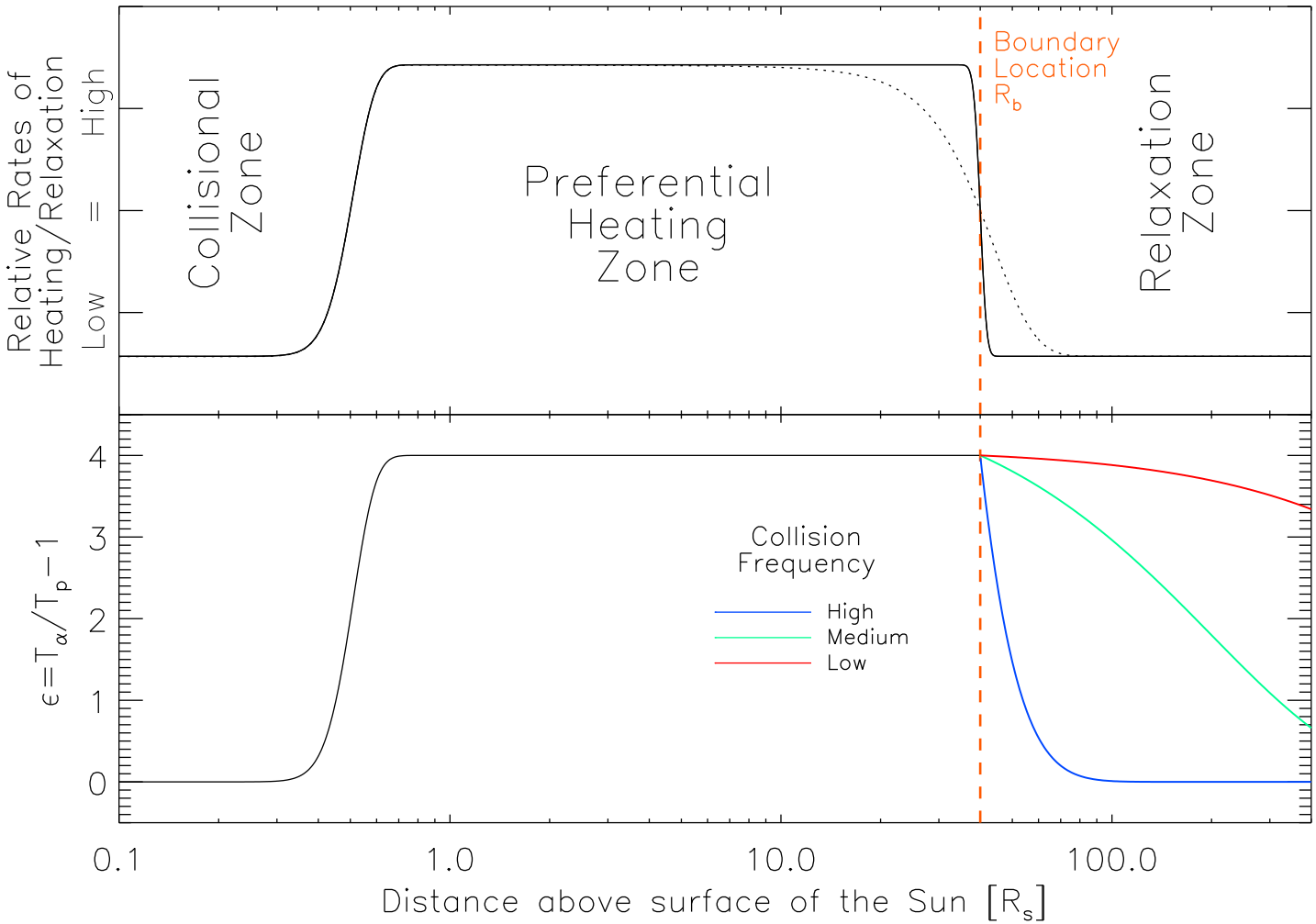

$\epsilon = T_\alpha/T_p - 1$ reaches an equilibrium value within the zone, and then relaxes as the solar wind expands.

Describing the Excess Temperature $\epsilon \equiv T_\alpha/T_p - 1$

We model the radial evolution of T_p and T_α as

$$\frac{dT_s}{dr} = (\gamma - 1)\left[\frac{T_s}{n_s}\frac{dn_s}{dr} - \frac{Q_s}{n_s k_B U}\right] - \sum_{s'}\frac{\nu_{ss'}}{U}(T_s - T_{s'})$$

If no **preferential** heating occurs beyond R_b (e.g. $Q_\alpha = Q_p \frac{n_\alpha T_\alpha}{n_p T_p}$ **or** $Q_s = 0$), we write

$$\frac{d\epsilon}{dr} = -\epsilon\left[\frac{\nu_{\alpha p}}{U} + \frac{\nu_{p\alpha}}{U}(\epsilon + 1)\right]$$

This results in a differential equation of the form:

$$\int_{R_b}^{R_w} \frac{2}{5}\frac{\left[1 + \frac{(\epsilon+1)}{4}\right]^{3/2} d\epsilon}{\epsilon(1+F) + \epsilon^2 F} = -\int_{R_b}^{R_w} \frac{\tilde{\nu}_{\alpha p}(r)}{U(r)} dr \equiv -A_c$$

The right-hand side is simply a sophisticated collisional age:

$$-\int_{R_b}^{R_w} \frac{\tilde{\nu}_{\alpha p}(r)}{U(r)} dr \equiv -A_c$$

with $\frac{\nu_{p\alpha}}{\nu_{\alpha p}} = \frac{n_\alpha m_\alpha}{n_p m_p} \equiv F$,

$\nu_{ss'} = 4\pi q_s^2 q_{s'}^2 \frac{\ln\Lambda n_{s'}}{m_s \mu w_{ss'}^3}$ (Hernandez & Marsch 1987) and

$$\tilde{\nu}_{ss'} = 8\pi q_s^2 q_{s'}^2 \frac{\ln\Lambda n_{s'}}{m_s^2 w_{s'}^3} = \frac{2\nu_{ss'}}{1 + m_s/m_{s'}} \left(1 + \frac{T_s m_{s'}}{T_{s'} m_s}\right)^{3/2}$$

The left-hand side 'simplifies' to:

$$\int_{R_b}^{R_w} \frac{2}{5} \frac{\left[1 + \frac{(\epsilon+1)}{4}\right]^{3/2} d\epsilon}{\epsilon(1+F) + \epsilon^2 F} = \frac{1}{10} \frac{\sqrt{5+\epsilon_w} - \sqrt{5+\epsilon_0}}{F}$$

$$- \frac{\sqrt{5}}{2(1+F)} \left[\frac{1}{2} \ln\left(\frac{\sqrt{1+\frac{\epsilon_w}{5}}+1}{\sqrt{1+\frac{\epsilon_w}{5}}-1}\right) - \frac{1}{2} \ln\left(\frac{\sqrt{1+\frac{\epsilon_0}{5}}+1}{\sqrt{1+\frac{\epsilon_0}{5}}-1}\right)\right]$$

$$+ \frac{(4F-1)^{3/2}}{10F^{3/2}(1+F)} \left[\tanh^{-1}\left(\frac{\sqrt{F}\sqrt{5+\epsilon_w}}{\sqrt{4F-1}}\right) - \tanh^{-1}\left(\frac{\sqrt{F}\sqrt{5+\epsilon_0}}{\sqrt{4F-1}}\right)\right]$$

Example Fits to Wind Data

For 25 km s^{-1} solar wind speed bins and fixed solar wind temperature and density radial trends, we fit
1) ϵ in the zone ϵ_0
2) residual ϵ when fully relaxed, ϵ_w, and
3) R_b
using Wind observations organized by Coulomb Age A_c

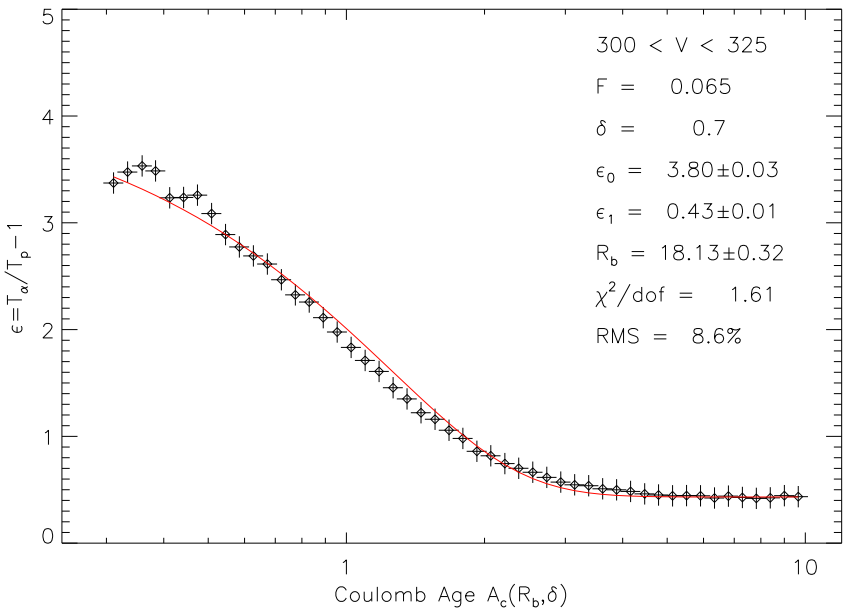

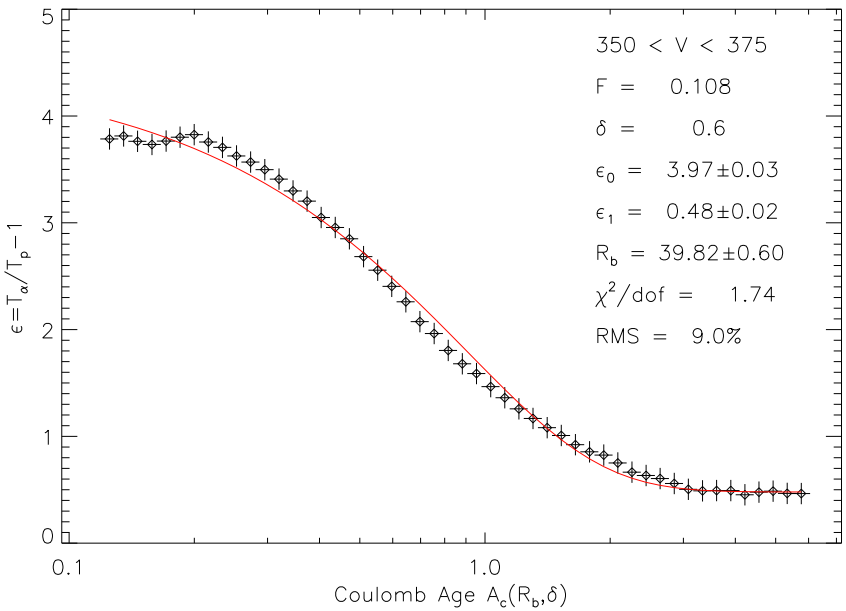

- Our model predicts ϵ to within $\sim 8\%$ of observational values with χ^2/dof~ 1.7.

Is there an Equilibrium ϵ in the Zone?

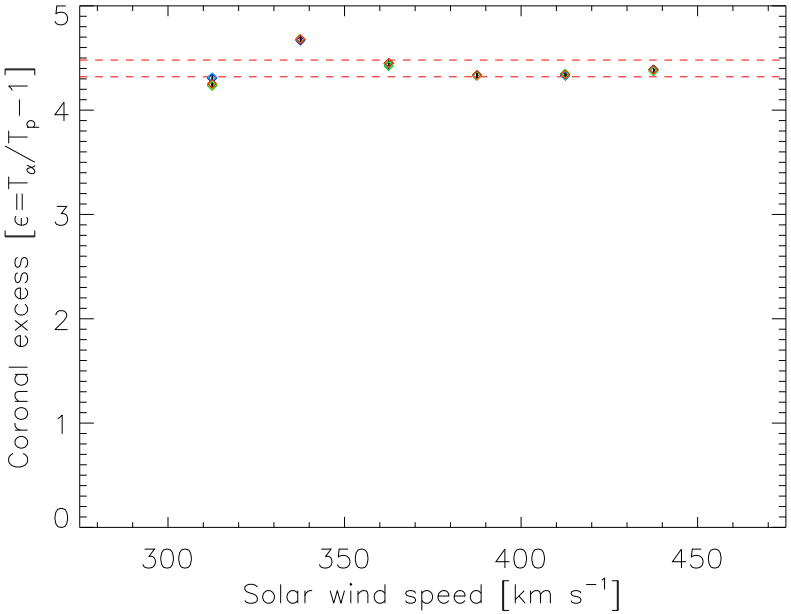

Kasper et al 2017 Wind

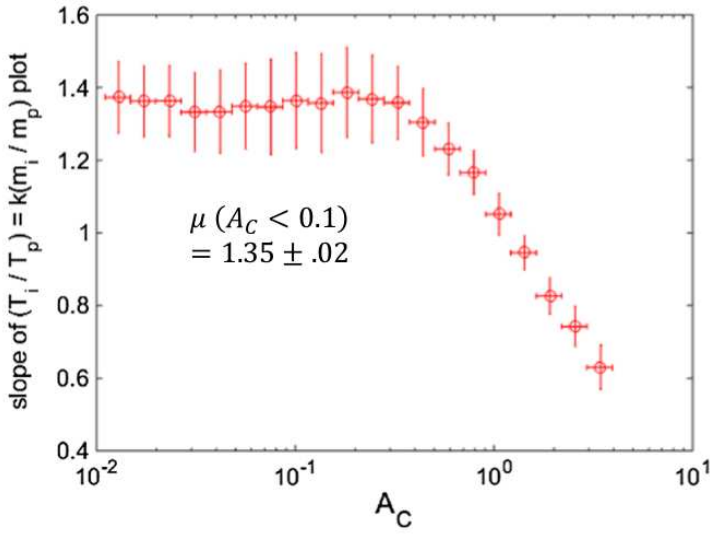

Tracy et al 2016 ACE

Regardless of wind speed and radial temperature trends, the excess temperature ratio $T_\alpha/T_p \approx 5.5$.

This agrees with heavier minor ion observations at 1 AU, which predict that collisionless minor ions should have $T_i/T_p = 1.35 m_i/m_p$.

Does the Zone Move?

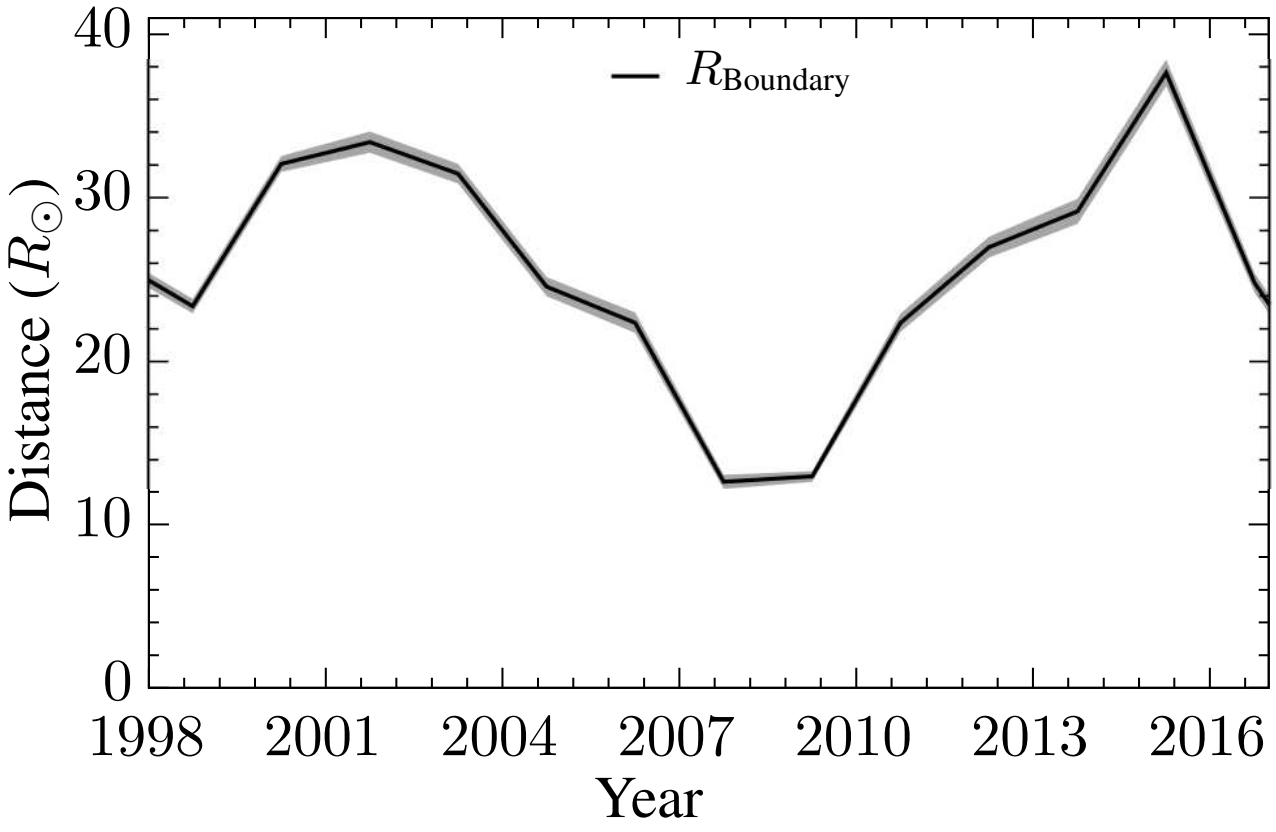

Kasper & Klein 2019

Using the same analysis, but dividing into 1.5 year intervals, we time dependent motion of R_b

Does the Zone Correspond to Solar Activity?

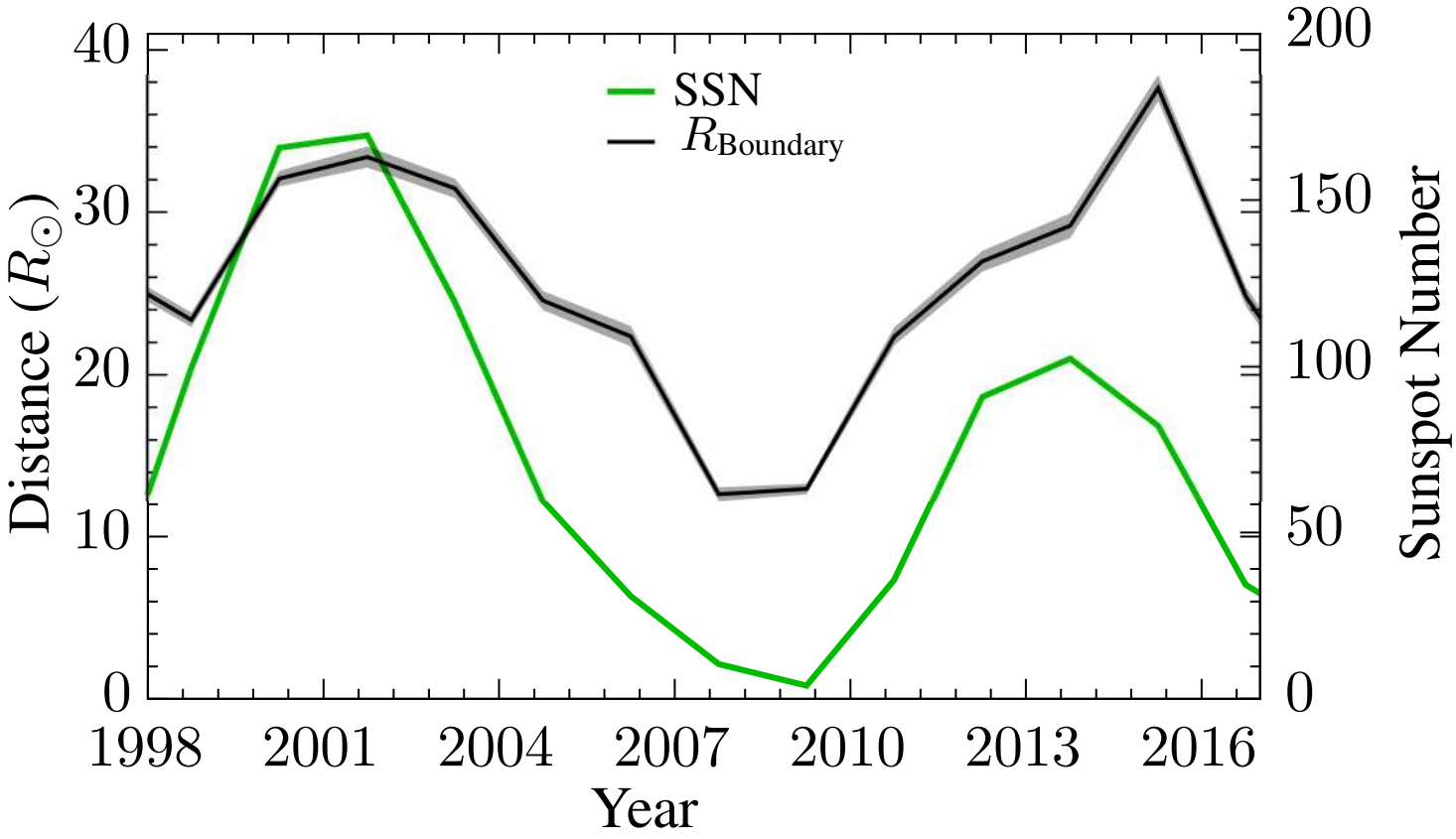

Kasper & Klein 2019

R_b is correlated with SSN ~ 0.84, indicating some connection to the solar cycle.

Does the Zone Correspond to a Characteristic Distance?

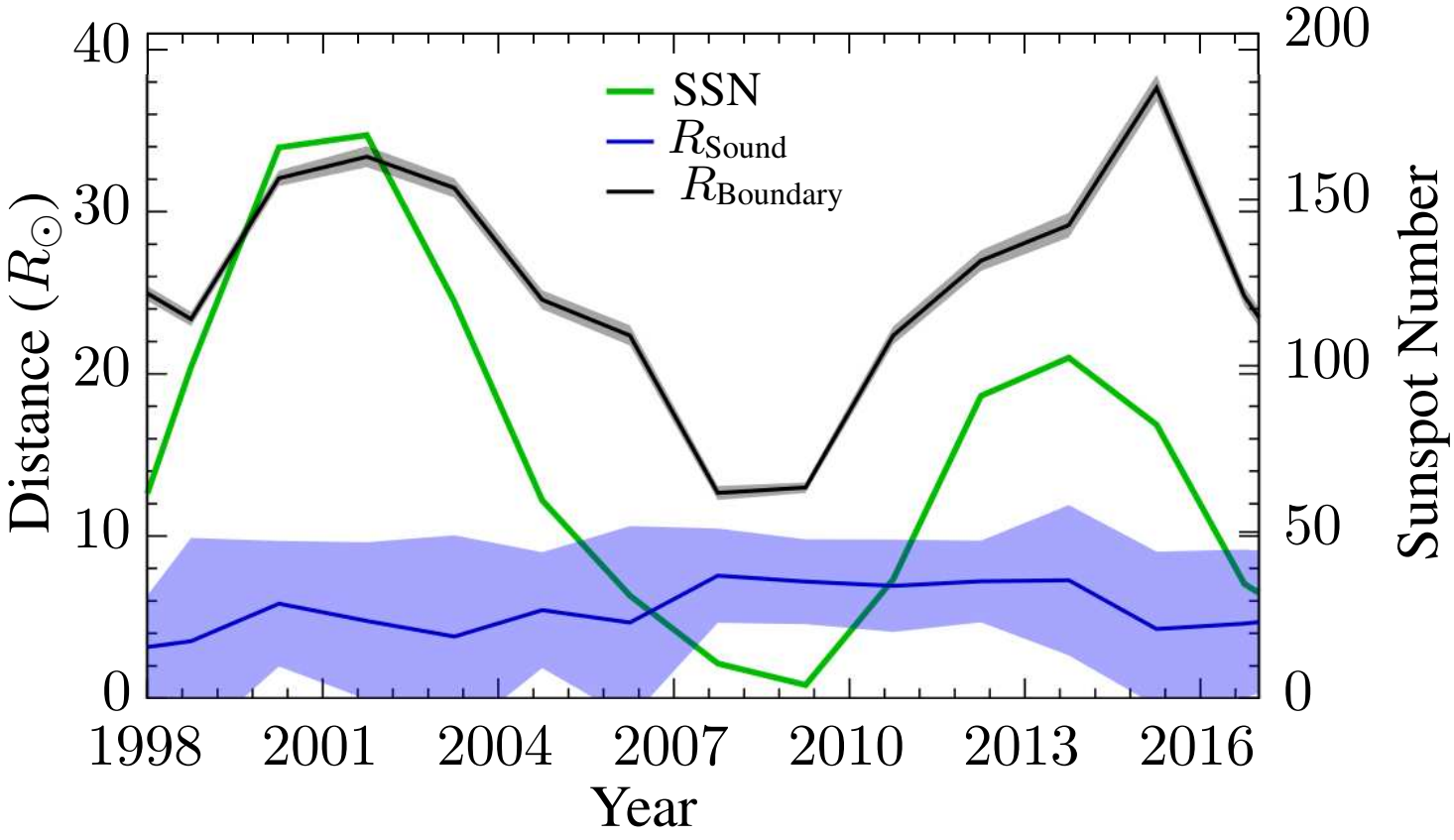

Kasper & Klein 2019

R_b is not well correlated with R_{sound} (~ -0.35).

Does the Zone Correspond to a Characteristic Distance?

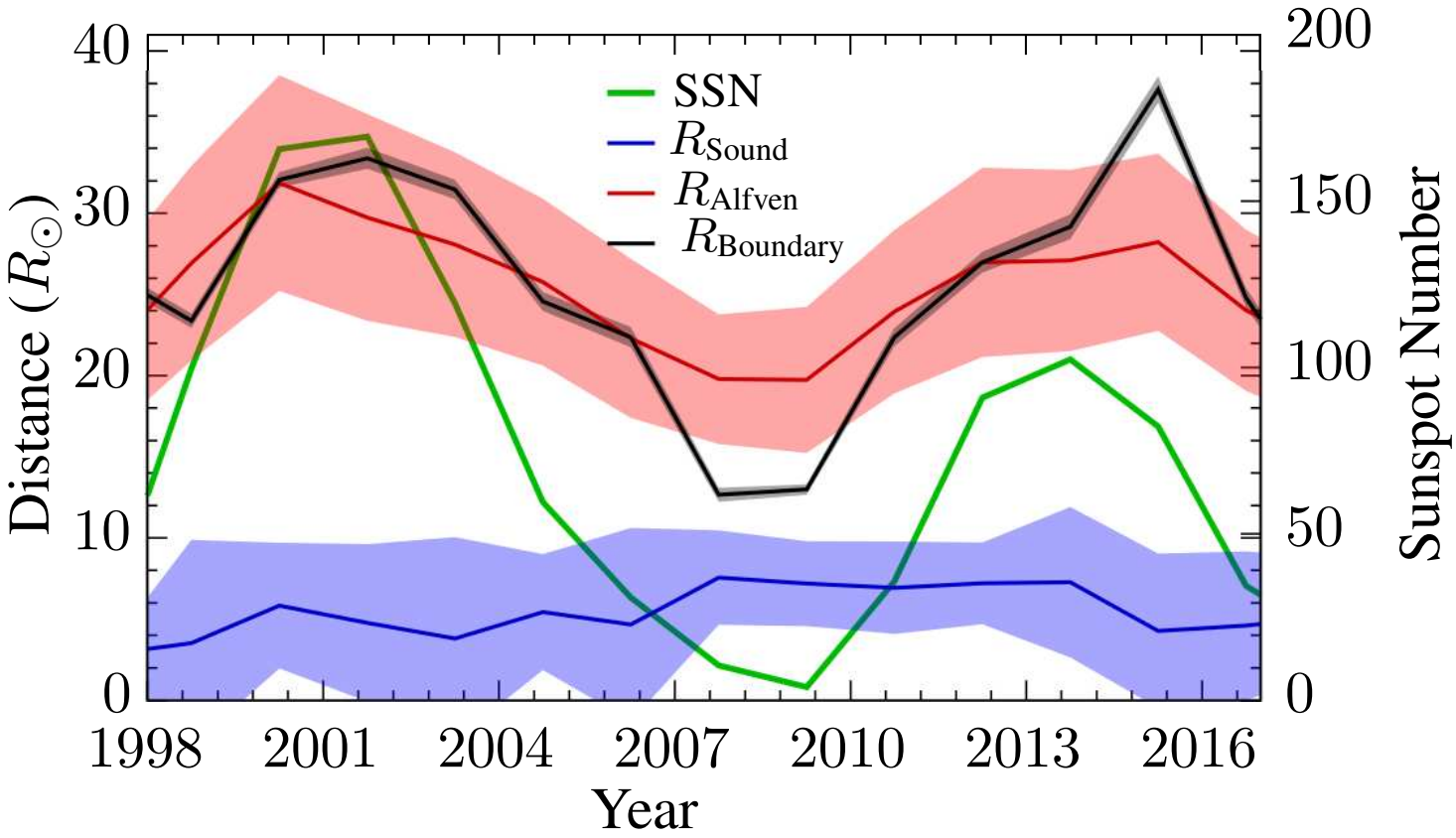

Kasper & Klein 2019

R_b is best correlated with the Alfvén surface (~ 0.95). This correlation holds regardless of the choice of radial exponents for U and T.

When will we sample the preferential heating regime?

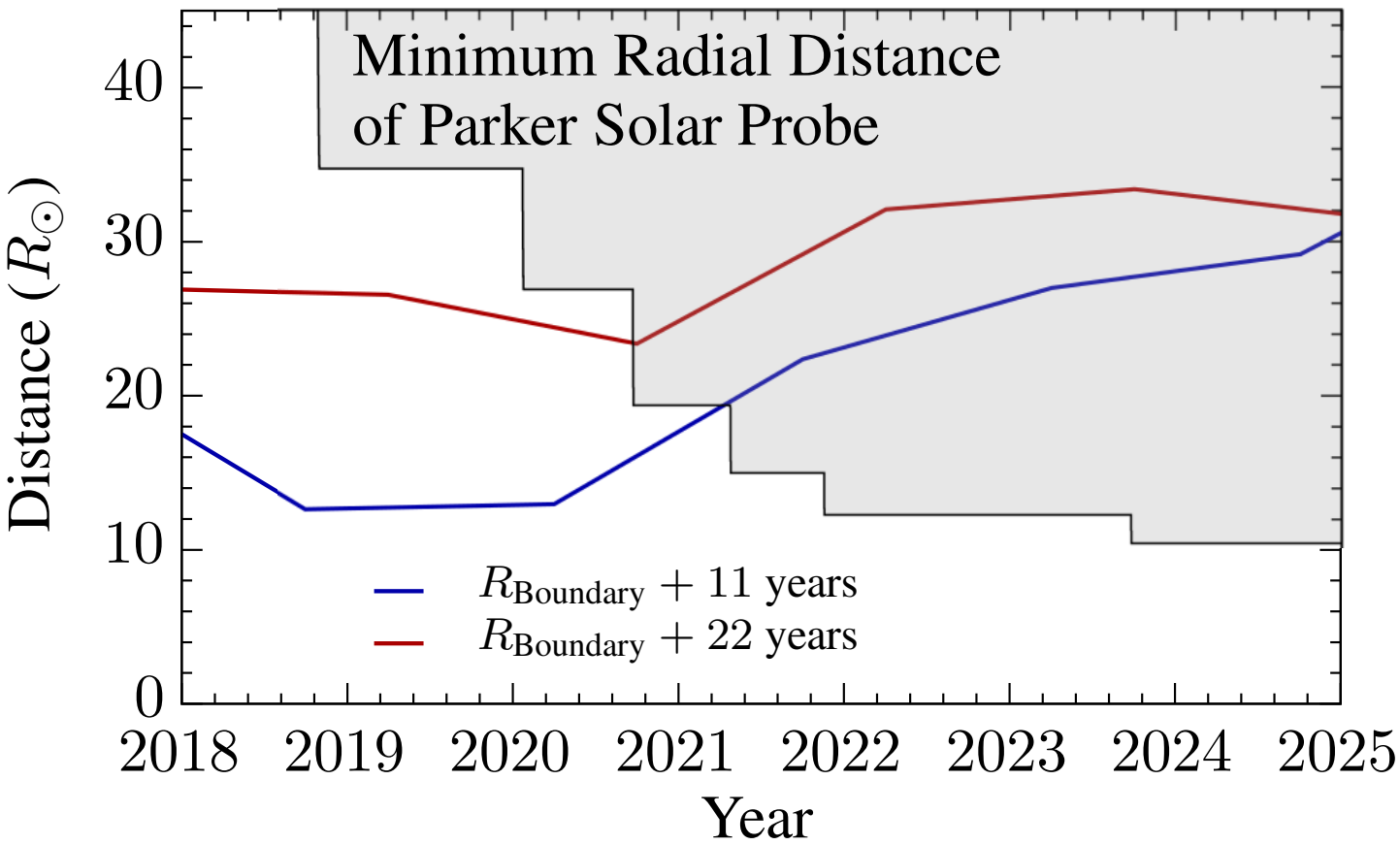

Kasper & Klein 2019

Based upon this model, we predict that the first in situ measurement of this preferential heating mechanism will be by PSP and will occur in 2020-2021.

Parker Solar Probe: NASA's mission to 'touch the Sun'

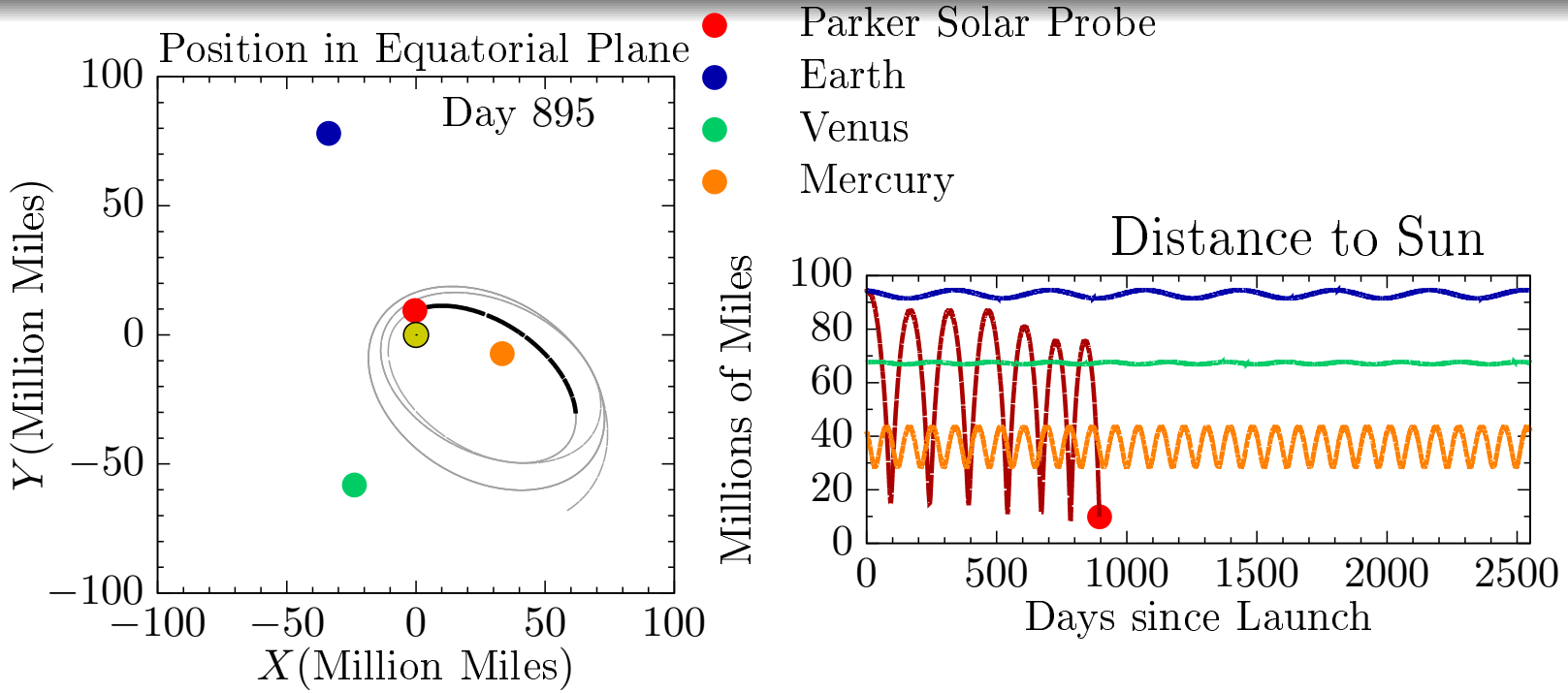

PSP will measure the local plasma (SWEAP) and E/M fields (FIELDS) at distances closer to the Sun than any previous mission.

One of the principle objectives is to "[t]race the flow of energy that heats the solar corona and accelerates the solar wind."

If interested in becoming familiar with SWEAP/Fields data formats, inquire about Working Groups.

Data becomes public November 11.

"It is of the nature of idea to be communicated: written, spoken, done. The idea is like grass. It craves light, likes crowds, thrives on crossbreeding, grows better for being stepped on."— *The Dispossessed* Ursala K. Le Guin